J Ther Eng, Vol. 10, No. 1, pp. 219−243, January, 2024

Journal of Thermal Engineering
Web page info: https://jten.yildiz.edu.tr
DOI: 10.18186/thermal.1429974

Journal of Thermal Engineering

Research Article

Multi-objective optimization of a biomass microCHP-ORC system under supercritical conditions

Panagiotis KLADISIOS[1,*], Athina SAGIA[1]

[1]*Laboratory of Heat Transfer and Thermal Processes, School of Mechanical Engineering, National Technical University of Athens, 9 Iroon Polytechniou Str., Zografou 15780, Greece*

ARTICLE INFO

Article history
Received: 05 July 2022
Accepted: 13 August 2022

Keywords:
ORC; Supercritical; CHP; Biomass, Parametric Analysis; Multi-Objective Optimization; Genetic Algorithm; R124; Isobutane; R245fa; Isopentane

ABSTRACT

ORC cycle is one of the most efficient technologies for the utilization of low-grade heat. ORC systems cover a wide range of heat sources and power outputs. Apart from increasing the overall efficiency, CHP systems contribute to the decentralization of energy production, the conservation of primary fuel, the reduction of the emission of greenhouse gasses and the reduction of the cost to the final consumer. This justifies the research activity around CHP-ORC systems. In the present paper, a steady-state thermodynamic model for a 50 kW_{el} biomass microCHP-ORC was developed and four candidate fluids were selected: R124, isobutane, R245fa and isopentane. The multi-objective optimization under supercritical conditions was performed using the genetic algorithm. The thermal efficiency, the exergy efficiency and the total heat exchanger surface were selected as single objectives. The evaporation temperature and pressure and the pinch point temperature differences at the heat exchangers were selected as decision variables. Careful examination of the optimal results revealed a systematic tendency for high evaporation temperatures and pressures and low recuperator pinch point temperature differences. Recuperation was found beneficial in many aspects, especially at higher evaporation temperatures. Also, the use of cogeneration leads to overall system efficiencies that surpass 90%, while simultaneously saving at least 20% fuel. Lastly, isopentane was found to be the best-performing fluid.

Cite this article as: Kladisios P, Sagia A. Multi-objective optimization of a biomass micro-CHP-ORC system under supercritical conditions. J Ther Eng 2024;10(1):219−243.

INTRODUCTION

Organic rankine cycle is considered as a reliable technology for the efficient conversion of low temperature heat into electrical power [1]. Conventional technologies are unsuitable for this purpose, with Kalina cycle being the only viable alternative [2]. The most common sources of low-grade heat are solar and geothermal energy, biomass and waste heat from industrial activities [3-4].

The working principle of an ORC cycle is similar to that of the conventional water-steam Rankine cycle. Their most significant difference lies in the working fluid. The conventional Rankine cycle uses water. It is cheap, abundant,

*Corresponding author.
*E-mail address: pkladisios@central.ntua.gr

This paper was recommended for publication in revised form by Müslüm Arıcı

thermochemically stable, non-flammable and non-corrosive. Furthermore, it has high normal boiling point (NBP), high critical temperature (373.95 °C) and low molecular weight. At the same time, water is associated with serious drawbacks. In a steam turbine cycle, a significant amount of superheating is required in order to avoid expansion at the two-phase region and the consequent turbine blade erosion. In addition, steam turbines are generally linked with more complex and expensive installations. ORC systems use organic fluids with higher molecular weights and lower normal boiling points [4-7]. ORC cycle is suitable for the utilization of heat sources with temperatures up to 300 °C. At higher temperatures the conventional Rankine cycle is more efficient [8]. ORC is considered as a proven viable technology for decentralized applications and power from a few kW_{el} up to 1 MW_{el} [1].

Despite their advantages, ORC systems suffer from low thermal efficiencies, due to the low temperature levels of the heat sources [5, 8]. Their optimization is, therefore, of paramount importance. It is indicative that a large portion of the pertinent literature is focused on the development of methods for the selection of suitable working fluids and optimal working conditions [9-10].

In some types of problems, the optimization is a simple process, since the achievement of a single target is sufficient (Single Objective Optimization, SOO). However, in most real applications many criteria (objective functions) have to be met, which may be competitive to each other. This is the subject of multi-objective optimization (MOO) [8]. The single objectives include a great number of thermodynamic, financial and environmental indices such as thermal efficiency, exergy efficiency and net produced power. One of the most common approaches to the multi-objective optimization of ORC systems is the genetic algorithm (Genetic Algorithm, GA) [9-10].

GA is inspired by the biological evolution and specifically from the concepts of natural selection, heredity and mutation. It stands out for its ability to handle complex optimization problems and large numbers of variables. It tracks universal optima, even with the presence of multiple local optima. In comparison with other search methods, it is less dependent on the initial conditions [11-12]. A significant portion of the literature concerning the multi-objective optimization of ORC systems is devoted solely to genetic algorithms [14-16].

In the present paper a steady-state thermodynamic model is developed and 4 candidate working fluids are selected, based on desired properties: R124, isobutene (R600a), R245fa and isopentane (R601a). The multi-optimization with a simple genetic algorithm follows. Thermal efficiency, exergy efficiency and total heat exchanger surface are the single objectives, whose combination formulates the fitness function. The problem was programmed and solved in Python codes, developed by the writers.

An essential difference with other approaches pertains to the pinch point of the heat exchangers. The pinch point of a heat exchanger is the position, where the temperature difference between the two streams receives its lowest value. This difference is called PPTD (Pinch Point Temperature Difference) and is an important design and operating parameter of an exchanger. It affects the efficiency as well as the cost of the system. Lower PPTD values lead to a more efficient exchanger. At the same time, the required surface and consequently the cost are increased. Higher PPTD values are associated with elevated heat losses to the environment. In practice, the pinch point temperature difference is usually the one recommended by the manufacturer. Alternatively, it is the result of an optimization process. In most theoretical cases, a specific PPTD value is assumed for each exchanger [17-19]. This paper includes the pinch point temperature differences in the vector of the decision variables of the genetic algorithm. For a given inlet temperature, the exit temperature and mass flow of the thermal oil and water are adjusted through pinch point analysis, in order to achieve the PPTD value that is required each time.

The multi-objective optimization revealed isopentane as the best-performing fluid. In addition, the concepts of cogeneration and recuperation reduce biomass fuel consumption and are beneficial to the overall efficiency of the system.

ORGANIC RANKINE CYCLE

The basic components of an ORC cycle are: pump, evaporator, expander and condenser. In cases where the temperature at the expander exit is sufficiently high, an internal heat exchanger (IHE) known as the recuperator can be used to increase the thermal efficiency of the cycle. Preheating the cold stream through a recuperator improves the thermal efficiency of the cycle, because the same amount of work is produced using less heat input [20-21]. Depending on the presence of an internal heat exchanger, ORC cycles can be conventional or recuperative [22,23].

In an ideal Rankine cycle there are no pressure loses in the evaporator, condenser and piping. There is also no heat exchange between the components and the environment. Furthermore compression and expansion are considered to be isentropic processes. Thus, a working fluid in an ORC system undergoes the following processes:

Process 1-2 (pump): Isentropic compression from condenser to evaporator pressure. Fluid enters the compressed liquid region.

Process 2-3 (evaporator): Isobaric heating in the evaporator. Depending on the cycle type, the fluid becomes saturated or superheated vapor or it may enter the supercritical state.

Process 3-4 (expander): Isentropic expansion from evaporator to condenser pressure. Fluid may be in the superheated state or in the two-phase liquid-vapor region.

Process 4-1 (condenser): Isobaric cooling in the condenser. Fluid reaches its original saturated liquid state [24].

An Organic Rankine Cycle can be classified into subcritical or supercritical, based on the state of the working fluid at the exit of the evaporator [20]. In Fig. 1 the types of ORC cycle are depicted in temperature versus specific entropy diagrams.

In the subcritical ORC the working fluid at the exit of the evaporator may be at a state of saturated or superheated vapor. In the latter case, superheating is involved. Depending on the working fluid properties and the operating conditions, superheating may be linked to higher thermal efficiencies. The permissible degree of superheating, however, is usually small due to the low heat transfer coefficients of the vapor states. Excessive superheating is tantamount to larger and more expensive heat exchangers. Moreover, superheating is commonly used to avoid the two-phase liquid-vapor region during the expansion process. The presence of droplets is responsible for blade erosion and turbine efficiency reduction. Since in the case of most organic fluids the expansion ends at the superheated region, superheating becomes optional [1, 25].

In the case of a supercritical cycle, the fluid is vaporized from the compressed liquid state at the exit of the pump directly to a supercritical state before it is expanded. The fluid does not undergo phase change. In a supercritical ORC the average temperature of heat input is higher which leads to increased thermal efficiencies. In addition there is an improvement in the heat transfer between heat source and working fluid at the external heat exchanger [20]. At the same time, however, supercritical cycle increases the complexity and installation cost due to the high operating pressures [26].

MODELING

In the present paper a 50 kW_{el} biomass-fed micro-CHP-ORC will be examined. The schematic of the system is displayed in Fig. 2.

The combustion of biomass produces warm flue gases. Their heat is transferred to the working fluid indirectly, through a thermal oil loop [4]. This ensures the thermochemical stability of the working fluid. The present model is based on the following assumptions [28-31]:

- Steady-state operation.
- Negligible pressure losses in heat exchangers and piping.
- No heat transfer between components and environment.
- No changes in kinetic and dynamic energy.
- Constant isentropic efficiencies in expander and pump.
- Negligible consumed power by the thermal oil and water pumps.
- Constant electromechanical losses in the expander-generator coupling.
- Negligible variations of specific heat under constant pressure versus temperature.

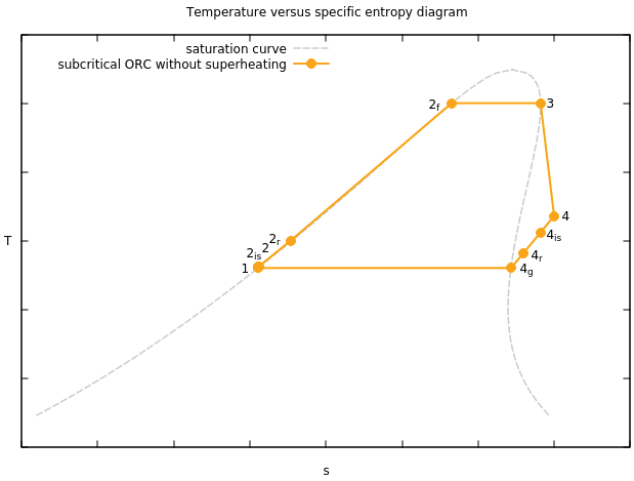

(a)

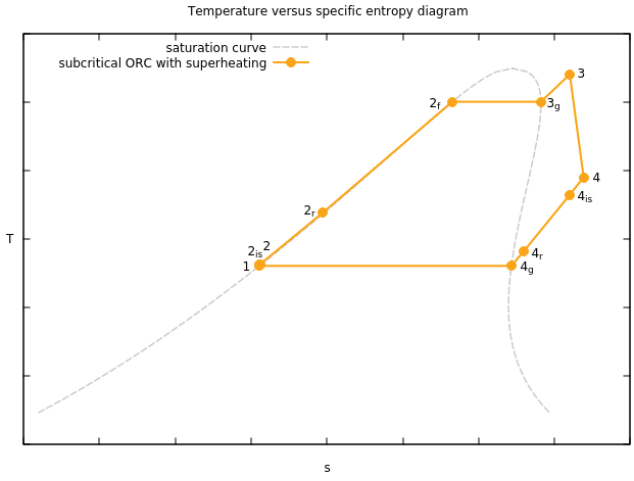

(b)

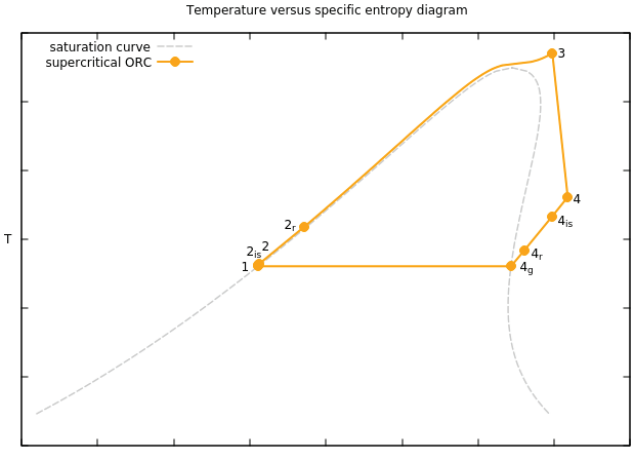

(c)

Figure 1. Types of ORC cycles: subcritical without superheating (a), subcritical with superheating (b) and supercritical (c).

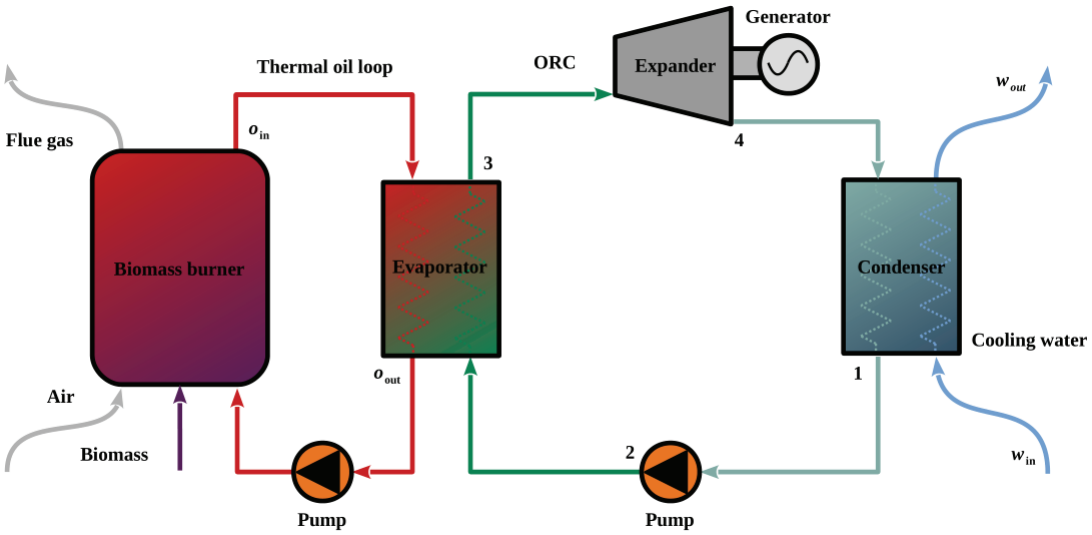

(a)

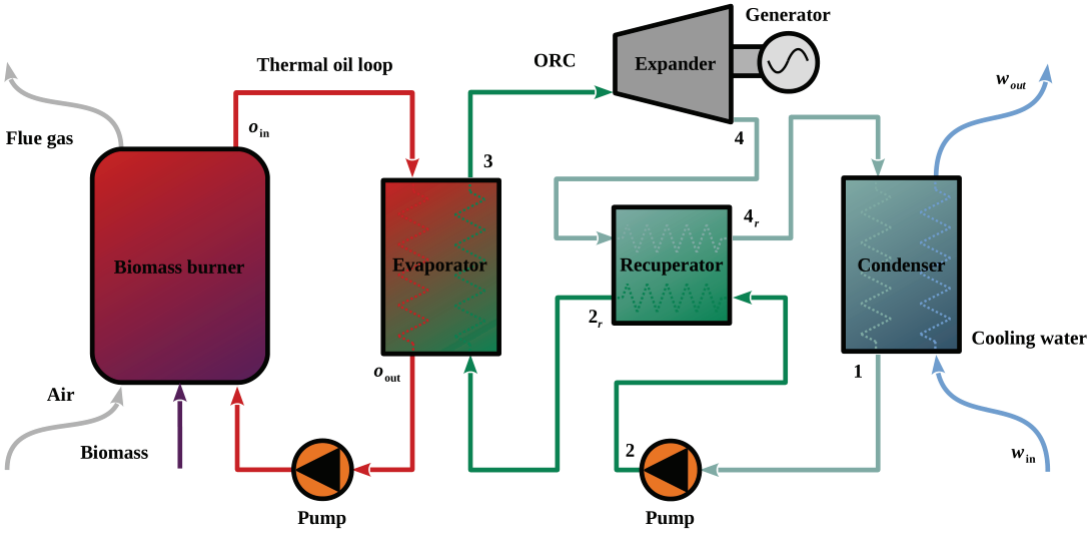

(b)

Figure 2. Typical biomass CHP-ORC configurations: (a) without internal heat exchanger and (b) with internal heat exchanger.

System Description

The equations that describe the components of the system are derived from the conservation of mass and energy and the entropy and exergy balance in a closed volume [24, 32].

The power consumed by the pump is:

$$\dot{W}_p = \dot{m}_{wf} w_p = \dot{m}_{wf}(h_2 - h_1) \tag{1}$$

The pump isentropic efficiency is defined thusly:

$$n_{is,p} = \frac{(h_{2is} - h_1)}{(h_2 - h_1)} \tag{2}$$

The rate of exergy destruction in the pump is:

$$\dot{E}_{xd,p} = \dot{m}_{wf} T_0 (s_2 - s_1) \tag{3}$$

where T_o represents the temperature in the dead state (temperature of the environment).

The heat absorbed by the evaporator is:

$$\dot{Q}_{evap} = \dot{m}_{wf} q_{evap} = \dot{m}_{wf}(h_3 - h_2) \quad (4)$$

The rate of exergy destruction in the evaporator can be calculated by the following equation:

$$\dot{E}_{xd,evap} = \dot{m}_{wf} T_0 \left[(s_3 - s_2) - \frac{(h_3 - h_2)}{T_o}\right] \quad (5)$$

where T_o is the average thermal oil temperature. Specifically:

$$T_o = \frac{(T_{o,in} + T_{o,out})}{2} \quad (6)$$

The power produced by the expander can be calculated by:

$$\dot{W}_e = \dot{m}_{wf} w_e = \dot{m}_{wf}(h_3 - h_4) \quad (7)$$

The corresponding isentropic efficiency is defined as follows:

$$n_{is,e} = \frac{(h_3 - h_4)}{(h_3 - h_{4is})} \quad (8)$$

The rate of exergy destruction in the expander can be calculated with the following equation:

$$\dot{E}_{xd,e} = \dot{m}_{wf} T_0 (s_4 - s_3) \quad (9)$$

The heat rejected by the condenser is:

$$\dot{Q}_{cond} = \dot{m}_{wf} q_{cond} = \dot{m}_{wf}(h_4 - h_1) \quad (10)$$

The rate of exergy destruction in the condenser is:

$$\dot{E}_{xd,cond} = \dot{m}_{wf} T_0 \left[(s_1 - s_4) - \frac{(h_1 - h_4)}{T_w}\right] \quad (11)$$

where T_w is the average water temperature:

$$T_w = \frac{(T_{w,in} + T_{w,out})}{2} \quad (12)$$

The net power produced by the cycle is:

$$\dot{W}_{net} = \dot{W}_e - \dot{W}_p \quad (13)$$

The thermal efficiency of the cycle is defined as the ratio of the net power to the heat input of the cycle:

$$n_{th} = \frac{\dot{W}_{net}}{\dot{Q}_{evap}} = \frac{w_{net}}{q_{evap}} = \frac{(h_3 - h_4) - (h_2 - h_1)}{(h_3 - h_2)} \quad (14)$$

The heat recovered by the internal heat exchanger is:

$$\dot{Q}_{rec} = \dot{m}_{wf}(h_4 - h_{4r}) = \dot{m}_{wf}(h_{2r} - h_2) \quad (15)$$

and the corresponding rate of exergy destruction can be expressed as follows:

$$\dot{E}_{xd,rec} = \dot{m}_{wf}[(h_4 - h_{4r} + h_2 - h_{2r}) - T_0(s_4 - s_{4r} + s_2 - s_{2r})] \quad (16)$$

In the case of an internal heat exchanger, states 2 and 4 are replaced by states 2*r* and 2*r* respectively. This has to be reflected in the equations for the evaporator and condenser, as well as for the thermal efficiency.

The calculation of the working fluid mass flow rate is based on the required power output. Assuming that the expander-generator coupling has efficiency n_{em}, the relationship between power output and net power is:

$$\dot{W}_{el} = n_{em} \dot{W}_{net} \quad (17)$$

Net power and specific net work are related by the following equation:

$$\dot{W}_{net} = \dot{m}_{wf} w_{net} \quad (18)$$

In a cogeneration system, the electrical efficiency is defined as the ratio of the produced electrical power to the power, which is introduced into the system:

$$n_{el,chp} = \frac{\dot{W}_{el}}{\dot{E}_{in}} \quad (19)$$

Accordingly, the thermal efficiency of a cogeneration system is defined as the ratio of the heat produced by the system to the heat that is introduced to it:

$$n_{th,chp} = \frac{\dot{Q}_{th}}{\dot{E}_{in}} \quad (20)$$

The heat produced by the CHP system is essentially the heat, which the condenser rejects.

The total cogeneration efficiency is defined as the ratio of the total produced power to the power input:

$$n_{chp} = \frac{\dot{W}_{el} + \dot{Q}_{th}}{\dot{E}_{in}} = n_{el,chp} + n_{th,chp} \quad (21)$$

The power input of the cogeneration system is the heat inserted in the form of biomass:

$$\dot{E}_{in} = \dot{Q}_{bm} = \dot{m}_{bm} LHV_{bm} \quad (22)$$

where $\dot{m}_{bm}$ the mass flow rate and LHV_{bm} the lower heating value of biomass.

By considering a constant boiler efficiency n_{boiler}, the heat that is absorbed by the thermal oil loop, and, consequently, by the evaporator is:

$$\dot{Q}_{evap} = n_{boiler}\dot{E}_{in} \quad (23)$$

The exergy efficiency is the ratio of the rate of output exergy to the rate of input exergy:

$$n_{ex,chp} = \frac{\dot{E}_{x,out}}{\dot{E}_{x,in}} = \frac{\dot{E}_{x,in}-\dot{E}_{xd,t}}{\dot{E}_{x,in}} = 1 - \frac{\dot{E}_{xd,t}}{\dot{E}_{x,in}} \quad (24)$$

where $\dot{E}_{xd,t}$ is the total rate of exergy destruction. The input exergy $\dot{E}_{x,in}$ is equal to the heat $\dot{Q}_{bm}$, that the biomass provides [33-37].

The PHR index (Power-to-Heat Ratio) is the ratio of the produced electrical power to the produced heat:

$$PHR = \frac{\dot{W}_{el}}{\dot{Q}_{th}} = \frac{n_{el,chp}}{n_{th,chp}} \quad (25)$$

The *PESR* index (Primary Energy Saving Ratio) reveals how much energy a cogeneration system conserves, in comparison to the systems that produce electrical power and heat separately. Is it defined as follows:

$$PESR = 1 - \frac{\dot{E}_{in}}{\frac{\dot{W}_{el}}{n_{el,ref}} + \frac{\dot{Q}_{th}}{n_{th,ref}}} = 1 - \frac{1}{\frac{n_{el,chp}}{n_{el,ref}} + \frac{n_{th,chp}}{n_{th,ref}}} \quad (26)$$

where $n_{el,ref}$ and $n_{th,ref}$ are the electrical and thermal efficiency of the reference systems. The typical values of $n_{el,ref}$ = 33% and $n_{th,ref}$ = 90% will be used [38-42].

Pinch Point Analysis

Pinch point analysis is used to determine the exit temperature and mass flow rate for the thermal oil and the water in the evaporator and the condenser respectively. In the case of the internal heat exchanger the exit states for both streams are determined. Given are the PPTD values, the inlet temperature and pressure of the thermal oil and the water, as well as the states of the ORC cycle. Each case will be explained in detail in the following sections.

Evaporator in supercritical conditions

In a supercritical cycle, due to the fact that the $T - \dot{Q}$ curve of the working fluid is non-linear, the location of the pinch point can be anywhere [43-44]. Thus, it has to be iteratively sought. A characteristic example is given in Fig. 3.

Given the thermal oil inlet temperature $T_{0,in}$ and the cycle states, suitable exit temperature $T_{o,out}$ and mass flow $\dot{m}_o$ of the thermal oil are sought, in order to achieve a given temperature difference, $\Delta T_{pp,evap}$.

By choosing an initial value of $T_{o,out}$ near $T_{0,in}$, the mean thermal oil temperature can be calculated:

$$T_o = \frac{1}{2}\left(T_{o,in} + T_{o,out}\right) \quad (27)$$

The corresponding specific heat capacity under constant pressure is:

$$C_{po} = C_{po}(T_o) \quad (28)$$

The total heat exchanged by the two streams is:

$$\dot{Q}_{evap} = \dot{m}_{wf}(h_3 - h_2) = \dot{m}_o C_{po}\left(T_{o,in} - T_{o,out}\right) \quad (29)$$

From Equation (29), the thermal oil mass flow can be calculated:

$$\dot{m}_o = \frac{\dot{m}_{wf}}{C_{po}}\frac{(h_3 - h_2)}{\left(T_{o,in} - T_{o,out}\right)} \quad (30)$$

The heat absorbed by the working fluid between state 2 and a random state *x* is:

$$\dot{Q}_{2\to x} = \dot{m}_{wf}(h_x - h_2) = \dot{m}_o C_{po}\left(T_{o,x} - T_{o,out}\right) \quad (31)$$

From the previous equation the thermal oil temperature $T_{o,x}$, which corresponds to position *x* of the working fluid can be calculated:

$$T_{o,x} = T_{o,out} + \frac{\dot{m}_{wf}}{\dot{m}_o}\frac{1}{C_{po}}(h_x - h_2) \quad (32)$$

This allows the calculation of the local temperature differences and, consequently, the calculation of the minimum. If the minimum temperature difference is greater than the desired value, the process is repeated for a decreased exit temperature, until the following criterion is met:

$$min\left[T_{o,x} - T_x\right] \le \Delta T_{pp,evap} \quad (33)$$

The presence of a recuperator affects the working fluid inlet. The working fluid is entering in state 2*r* and Equations (29)-(32) are expressed accordingly.

Internal heat exchanger

In the internal heat exchanger, the heat exchanged between the two streams is:

$$\dot{Q}_{rec} = \dot{m}_{wf}(h_4 - h_{4r}) = \dot{m}_{wf}(h_{2r} - h_2) \quad (34)$$

Since no phase change takes place, equation can be expressed as follows:

$$\dot{m}_{wf} C_{ph}(T_4 - T_{4r}) = \dot{m}_{wf} C_{pc}(T_{2r} - T_2) \quad (35)$$

Using the capacity rate definition:

$$C = \dot{m}c_p \quad (36)$$

Equation (35) can be rewritten as:

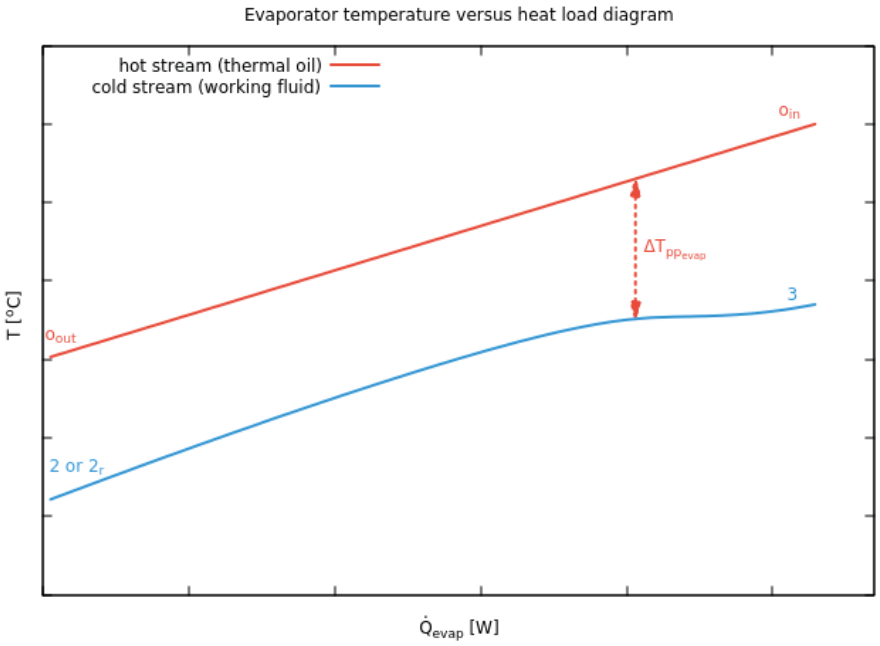

Figure 3. Temperature variation as a function of the thermal load and pinch point location for the evaporator under supercritical conditions.

$$C_h(T_4 - T_{4r}) = C_c(T_{2r} - T_2) \tag{37}$$

Due to the fact that, the hot stream is always vapor and the cold stream always fluid, the following is always true:

$$C_h < C_c \tag{38}$$

A direct conclusion of Equations (37) and (38) is that the temperature drop in the hot stream is always higher than the temperature rise in the cold stream. As a consequence, the minimum temperature difference of the two streams lies invariably on the hot stream exit (state 4*r*)/cold

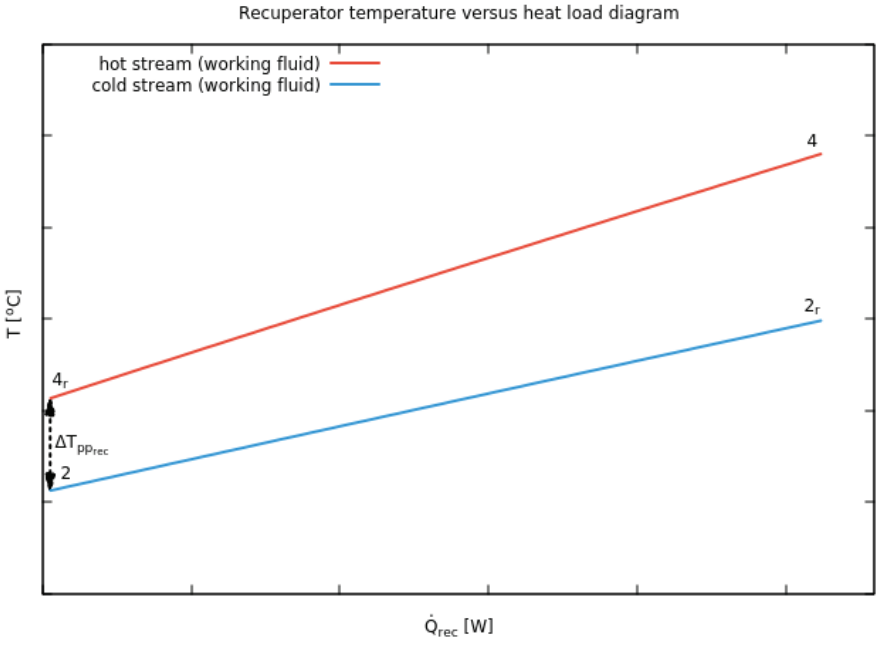

Figure 4. Temperature variation as a function of the thermal load and pinch point location for the internal heat exchanger.

stream entry (state 2). The relationship between temperatures T_{4r}, T_2 and the pinch point is:

$$T_{4r} = T_2 + \Delta T_{pp,reg} \quad (39)$$

Condenser

In contrast to the evaporator, the minimum temperature difference lies in a single position: at the start of the phase change of the working fluid (state 4*g*) [43-44]. Fig. 5 depicts the temperature as a function of thermal load of the condenser.

Given the water inlet temperature $T_{w,in}$, and the cycle states, the suitable water exit temperature $T_{w,out}$ and mass flow rate $\dot{m}_w$ are sought, in order to satisfy the desired pinch point temperature difference, $\Delta T_{pp,cond}$.

Similar to the case of the evaporator, the mass flow rate $\dot{m}_w$ and the exit temperature $T_{w,out}$ are determined iteratively. An initial value $T_{w,out}$ close to the inlet temperature $T_{w,in}$ is selected. The mean water temperature is:

$$T_w = \frac{1}{2}\left(T_{w,in} + T_{w,out}\right) \quad (40)$$

and the corresponding specific heat capacity under constant pressure is:

$$C_{pw} = C_{pw}(T_w) \quad (41)$$

The heat exchanged by the two streams is:

$$\dot{Q}_{cond} = \dot{m}_{wf}(h_4 - h_1) = \dot{m}_w C_{pw}\left(T_{w,out} - T_{w,in}\right) \quad (42)$$

From the previous equation, the water mass flow can be calculated:

$$\dot{m}_w = \frac{\dot{m}_{wf}}{C_{pw}} \frac{(h_4 - h_1)}{\left(T_{w,out} - T_{w,in}\right)} \quad (43)$$

The heat, that the working fluid absorbs between states 4 and 4*g*, is:

$$\dot{Q}_{4\to 4g} = \dot{m}_{wf}\left(h_4 - h_{4g}\right) = \dot{m}_w C_{pw}\left(T_{w,out} - T_{w,g}\right) \quad (44)$$

Therefore, the water temperature at the pinch point is:

$$T_{w,g} = T_{w,out} - \frac{\dot{m}_{wf}}{\dot{m}_w} \frac{1}{C_{pw}}\left(h_4 - h_{4g}\right) \quad (45)$$

If the temperature difference at the pinch point is higher than the desired value, the process is repeated by progressively increasing the exit temperature $T_{w,out}$, until the following condition is satisfied:

$$(T_{4g} - T_{w,g}) \leq \Delta T_{pp,cond} \quad (46)$$

Apparently, in the case of the recuperative cycle, state 4 is succeeded by state 4*r* in Equations (42)-(45).

Heat Exchanger Surface Calculation

The heat exchangers are assumed to be Plate Heat Exchangers (PHE). The surface calculation of the plate heat exchanger is directly affected by its geometry. Therefore, a brief description of the basic plate geometry must precede.

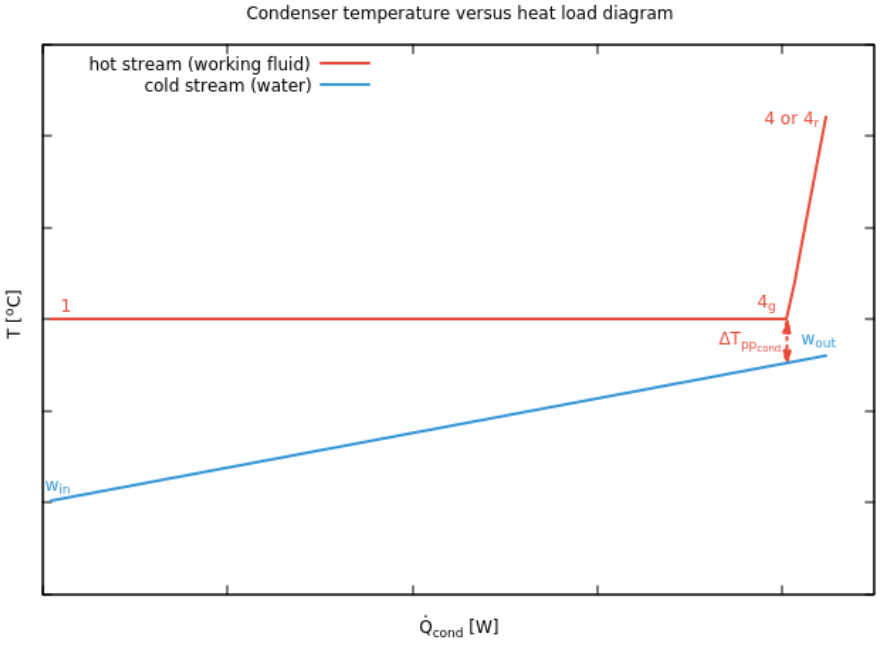

Figure 5. Temperature variation as a function of the thermal load and pinch point location for the condenser.

Plate heat exchanger geometry

In Fig. 6 the main geometric parameters of a chevron plate are depicted. Plate is characterized by the port diameter D_p, the horizontal distance, W_p and the vertical distance L_p between the ports. The plate section that participates in the heat transfer is defined by the effective length L_e and the effective width W_e. The corrugation geometry is characterized by the chevron angle β, the corrugation wavelength λ, the mean channel spacing b, the corrugation thickness t and the plate pitch p [45].

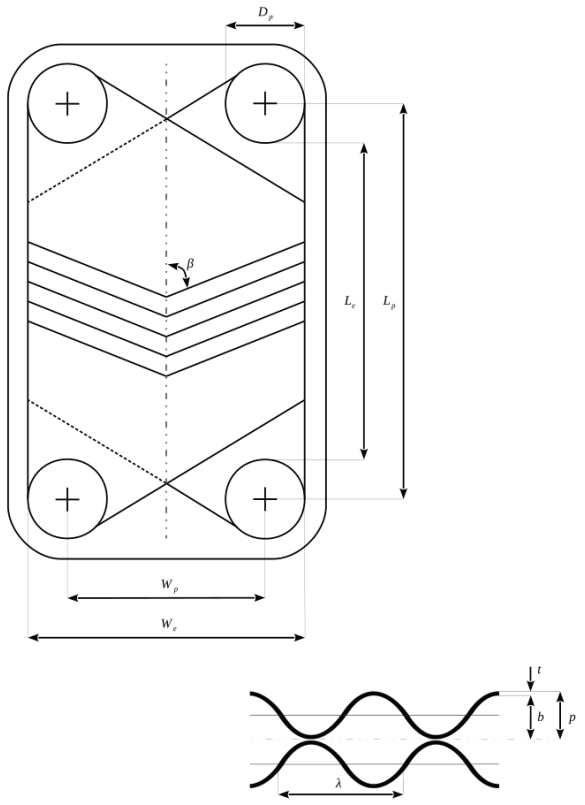

Figure 6. Geometric parameters of a chevron plate (adjusted from [45]).

The chevron angle β is the most influential and studied parameter. It affects the efficiency and the pressure drop of the exchanger. Typical values lie in the range 22° - 65°.

If the port diameter and the distance between the ports are known, the effective dimensions of the plate can be calculated by the following equations:

$$L_e = L_p - D_p \tag{47}$$

$$W_e = W_p + D_p \tag{48}$$

Thus, the projected surface of the plate is:

$$A_p = L_e W_e \tag{49}$$

The presence of corrugations increases the effective surface of the plate. This increase can be expressed by the enlargement factor, which is defined as:

$$\Phi = \frac{1}{6}\left(1 + \sqrt{1 + X^2 + 4\sqrt{1 + X^2/2}}\right) \tag{50}$$

The dimensionless parameter X is given by:

$$X = \frac{\pi b}{\lambda} \tag{51}$$

Typical values of Φ are between 1.15 and 1.25.

The effective surface of the plate can be calculated by the following equation:

$$A_e = \Phi A_p \tag{52}$$

The hydraulic diameter can be calculated as follows:

$$D_h = \frac{2b}{\Phi} \tag{53}$$

The mean channel spacing p can be estimated using the plate pitch p and corrugation thickness t:

$$b = p - t \tag{54}$$

Common values for b are within 2 - 5 mm. Despite the fact that, it is important for the heat transfer calculations, it is rarely provided by the manufacturer. In case where the p is unknown, b can be found indirectly, from the length of the compressed plate array, L_c:

$$p = \frac{L_c}{N_t} \tag{55}$$

In the previous equation N_t is the total number of plates.

The first and last plate do not contribute in the heat transfer. Therefore, the effective number of plates is:

$$N_e = N_t - 2 \tag{56}$$

Channel mass velocity (mass flow rate per unit of cross section surface) is derived from:

$$G = \frac{\dot{m}}{N_{cp} A_{ch}} \tag{57}$$

The number of channels per pass N_{cp} is:

$$N_{cp} = \frac{N_t - 1}{2N_p} \tag{58}$$

where N_p is the number of passes. A channel is the space between two consecutive plates. Pass is a group of channels that have the same flow direction.

The surface of a channel is calculated by:

$$A_{ch} = bL_e \tag{59}$$

Table 1. Geometric parameters for the chevron corrugation of a PHE [46-48].

Parameter	β [°]	b [m]	t [m]	p [m]	l [m]	D_h [m]	Φ [-]	A_{ch} [m^2]
Value	45	0.0020	0.0010	0.0030	0.0060	0.0032	1.2375	0.0013

Table 2. Geometric parameters and thermal conductivity for the plate of a PHE [46-48].

Parameter	W_p [m]	L_d [m]	W_e [m]	L_e [m]	D_p [m]	A_p [m^2]	A_e [m^2]	k [W/mK]
Value	0.4300	1.5500	0.6300	1.3500	0.2000	0.8505	1.0525	15

Tables 1-2 contain the geometric parameters of the chevron corrugation and the plate respectively, that are used. The selection was based on the typical ranges of the available literature [46-48].

LMTD method

The exchanger surface is calculated with the mean Logarithmic Mean Temperature Difference method (LMTD). According to this method, the exchanged heat can be expressed as follows:

$$\dot{Q} = UA\Delta T_{lm} \tag{60}$$

The logarithmic mean temperature difference can be calculated by:

$$\Delta T_{lm} = \frac{\Delta T_a - \Delta T_b}{ln\left(\frac{\Delta T_a}{\Delta T_b}\right)} \tag{61}$$

In the case of a counter-flow exchanger, the temperature differences ΔT_a and ΔT_b are defined:

$$\Delta T_a = T_{h,in} - T_{c,out} \tag{62}$$

$$\Delta T_b = T_{h,out} - T_{c,in} \tag{63}$$

With the heat flux $\dot{Q}$ and the inlet and outlet temperatures for both streams known, the calculation of the overall heat transfer coefficient U remains [32, 49].

Overall heat transfer coefficient

The overall heat transfer coefficient in Plate Heat Exchangers has been an object of studies for decades. A general theory or correlation capable of describing all possible combinations of geometric parameters and flow characteristics is unavailable, due to the complex nature of the problem. Its calculation is based on semi-empirical correlations for the Nusselt number [50-52].

In a plate heat exchanger, the overall heat transfer coefficient includes three discreet phenomena: convection of the hot fluid, convection of the cold stream and conduction in the interface between the two streams. By ignoring the thermal resistance due to fouling, the reciprocate of U is expressed thusly:

$$\frac{1}{U} = \frac{1}{a_h} + \frac{t}{k} + \frac{1}{a_c} \tag{64}$$

where t is the width and k the thermal conductivity of the interface. a_h and a_c are the convection coefficients for the hot and cold stream respectively.

In a forced convection, the Nusselt number equations are usually of the following form:

$$Nu = c_1 Re^{c_2} Pr^{c_3} \left(\frac{\mu_m}{\mu_w}\right) \tag{65}$$

where μ_m is the dynamic viscosity which corresponds to the mean temperature of the flow and μ_{wl} is the dynamic viscosity which corresponds to the wall temperature. Coefficients c_1, c_2 and c_3 depend on the plate geometry [52].

The Nusselt number is defined as the ratio of convective to conductive heat transfer at the boundary of a fluid:

$$Nu = \frac{a}{k/D_h} = \frac{aD_h}{k} \tag{66}$$

Hydraulic diameter is defined as:

$$D_h = \frac{4A}{P} \tag{67}$$

where A and P are the surface and perimeter of the cross section.

The Reynolds number is the ratio of inertial forces to the viscous forces within a fluid:

$$Re = \frac{uD_h}{\nu} = \frac{\rho u D_h}{\mu} = \frac{GD_h}{\mu} \tag{68}$$

The Prandtl number is defined as the ratio of momentum diffusivity to thermal conductivity:

$$Pr = \frac{\nu}{k/\rho C_p} = \frac{\mu/\rho}{k/\rho C_p} = \frac{C_p \mu}{k} \tag{69}$$

At this point, three temperatures, upon which the required calculations are based, must be explicitly defined. The mean or bulk temperature corresponds to the average temperature between the inlet and outlet temperature:

$$T_m = \frac{T_{in} + T_{out}}{2} \tag{70}$$

The plate temperature is the average temperature between the mean temperatures of the two streams:

$$T_{pl} = \frac{T_{m,h} + T_{m,c}}{2} \tag{71}$$

Lastly, the wall temperature on the side of a fluid is the average temperature between its mean temperature and the plate temperature [32, 46-47]:

$$T_{wl} = \frac{T_m + T_{pl}}{2} \tag{72}$$

Unless declared explicitly by the presence of the indices *pl* and *wl*, all properties are calculated based on the mean temperature T_m [53].

When phase change takes place, the temperature of a fluid remains constant. In these cases, properties are calculated based on the mean enthalpy between inlet and outlet [54]:

$$h_m = \frac{h_{in} + h_{out}}{2} \tag{73}$$

The following sections describe the Nusselt numbers correlations, that were selected for each heat transfer phenomenon.

Single-phase flow

In all cases of single phase-flow, the Kim is used, which is a function of the chevron angle [52, 55]:

$$Nu = \frac{hD_h}{k} = 0.295 Re^{0.64} Pr^{0.32} \left(\frac{\pi}{2} - \beta\right)^{0.09} \tag{74}$$

Supercritical region

In the supercritical region two zones are distinguished: subcritical and supercritical. In the supercritical zone, the typical equations cannot be used. The properties of a working fluid change rapidly, especially near the pseudocritical temperature. For a given supercritical pressure, the pseudocritical temperature T_{pcr} is the temperature that corresponds to the maximum specific heat capacity under constant pressure c_p [56-59].

The calculation of the Nusselt number takes place with the correlation proposed by Jackson and Hall, which takes the phenomenon into consideration and includes the pertinent correction [58-59]:

$$Nu = 0.0183 Re^{0.82} Pr^{0.5} \left(\frac{\rho_{wl}}{\rho}\right)^{0.2} \left(\frac{\overline{C_p}}{C_p}\right)^n \tag{75}$$

The average specific heat capacity, $\overline{C_p}$, is:

$$\overline{C_p} = \frac{h_{wl} - h_m}{T_{wl} - T_m} \tag{76}$$

Exponent *n* is estimated as follows:

$$\begin{aligned} &n = 0.4 \; for \; T_m < T_{wl} < T_{pcr} \; or \; 1.2T_{pcr} < T_m < T_{wl} \\ &n = 0.4 + 0.2\left(\frac{T_{wl}}{T_{pcr}} - 1\right) \; for \; T_m < T_{pcr} < T_{wl} \\ &n = 0.4 + 0.2\left(\frac{T_{wl}}{T_{pcr}} - 1\right)\left[1 - 5\left(\frac{T_m}{T_{pcr}} - 1\right)\right] \; for \; T_{pcr} < T_m < 1.2T_{pcr} \end{aligned} \tag{77}$$

Condensation

In a condenser two zones are observed: precooling or desuperheating and condensing zone.

The Nusselt number is calculated with Han, Lee and Kim correlation [52, 60]:

$$Nu = Ge_1 Re_{eq}^{Ge_2} Pr^{1/3} \tag{78}$$

The equivalent Reynolds number is defined as:

$$Re_{eq} = \frac{G_{eq} D_h}{\mu_f} \tag{79}$$

while, the equivalent mass velocity, G_{eq}, is given from:

$$G_{eq} = G\left[1 - x + x\left(\frac{\rho_f}{\rho_g}\right)^{0.5}\right] \tag{80}$$

The geometric parameters Ge_1 and Ge_2 are calculated by the following equations:

$$Ge_1 = 11.22\left(\frac{\lambda}{D_h}\right)^{-2.83}\left(\frac{\pi}{2} - \beta\right)^{-4.5} \tag{81}$$

$$Ge_2 = 0.35\left(\frac{\lambda}{D_h}\right)^{0.23}\left(\frac{\pi}{2} - \beta\right)^{1.48} \tag{82}$$

Number of plates

For the calculation of the total number of plates, and therefore of the required surface, the method described by Buonopane et al. is followed [46, 61]:

1. Estimation of inlet and outlet temperature for each stream.
2. Calculation of the exchanged heat $\dot{Q}$ and the logarithmic mean temperature difference ΔT_{lm} (Equation (61)).
3. Calculation of mass velocity G for N_{cp} = 1 (Equation (57)) and Reynolds number (Equation (68)) for each fluid.
4. Calculation of the convection coefficient for each fluid.
5. Calculation of the overall heat transfer coefficient U.
6. Estimation of the surface $A = \frac{\dot{Q}}{U\Delta T_{lm}}$ (Equation (60)).
7. Estimation of the total number of effective plates: $N_e = \frac{A}{A_p}$.

This methodology is appropriate when the inlet and outlet temperatures, the mass flow rates and the plate geometry are readily available.

Genetic Algorithm

Most variations of the genetic algorithm involve the following three operators: selection, crossover and mutation. Selection applies pressure to the population analogous to that of natural selection. The weaker individuals are gradually discarded, while the fitter have a higher chance of passing their genetic information on. Through crossover, solutions exchange information, similar to the way organisms reproduce. The offsprings have a combination of the genetic material of the parents. Selection and crossover are followed by mutation. Through mutation, new genetic information is introduced and thusly the diversity of the population is ensured. Mutation assists in avoiding local optima. Every time, the population undergoes these processes, the number of generations increases by 1.

In the present paper the simple genetic algorithm was implemented. The population of solutions has a real number representation and the parents were chosen through Tournament selection with a subgroup size of 2. The crossover method is the single-point crossover. The children replace the worst performing individuals at every generation. The algorithm ends after a predefined number of generations. The steps of the algorithm follow:

1. The algorithm initiates with the creation of a population of random solutions.
2. All individuals are evaluated based on their fitness value.
3. At the selection stage, the parents which are destined for the creation of offsprings are chosen.
4. Crossover results in the creation of offsprings, which replace the individuals of the population with the lowest fitness values.
5. Through mutation, all genes of the population have a small probability to mutate.
6. The algorithm ends when the termination criterion is met. Otherwise steps 2-5 are repeated.

It should be clarified that, the genetic algorithm does not provide a single optimal solution, but a set of non-dominated solutions that lie on the Pareto front. Problems of multi-objective optimization with conflicting objectives do not have a solution that satisfies all the criteria simultaneously.

The success of the algorithm depends strongly on the control parameters, i.e. the size of the population, the crossover and mutation probabilities and the number of parents and generations. Typical values for the population size and generations are 50 - 100 and 50 - 500 respectively. The crossover probability receives values usually 0.5 - 0.90, while the mutation probability in the range 0.001 - 0.1 [62-64]. Table 3 contains the values of the control variables that are used.

Table 3. Control parameters of the genetic algorithm

Parameter	Value
number of chromosomes	n_{chr} = 20
number of genes	n_{gn} = 4 or 5
crossover probability	p_c = 0.5
mutation probability	p_m = 0.05
number of parents	n_{par} = 4
maximum number of generations	n_{gener} = 50

Multi-objective function

A typical multi-objective problem is stated thusly:

$$\begin{gathered} minimize\ or\ maximize \\ F(\vec{X}) = [f_1(\vec{X}), f_2(\vec{X}), \dots, f_i(\vec{X}), \dots, f_k(\vec{X})]^T \\ g_j(\vec{X}) \le 0, j = 1,2, \dots, m \\ h_k(\vec{X}) = 0, l = 1,2, \dots, n \end{gathered} \quad (83)$$

where $F(\vec{X})$ is the multi-objective function and $\vec{X}$ decision variables vector. Functions $f_i(\vec{X})$ are the objectives, while functions $g_j(\vec{X})$ and $h_k(\vec{X})$ express the equality and inequality types of constraints respectively [65-66].

In the field of ORC optimization a plethora of thermodynamic, environmental and economic criteria are used. In the present paper, the thermal efficiency, the exergy efficiency and the total heat exchanger surface are selected as single objectives. The multi-objective function is the weighted sum of these single objectives (weighted sum method). Consequently, the aim of the optimization is the maximization of the following function:

$$F(\vec{X}) = w_1 f_1^{norm}(\vec{X}) + w_2 f_2^{norm}(\vec{X}) + w_3 f_3^{norm}(\vec{X}) \quad (84)$$

where f_1 is the thermal efficiency n_{th}, f_2 is the exergy efficiency n_{ex} and f_3 the total exchanger surface A_t.

Due to the fact the single objectives have different units and value ranges, a normalization is in order. The transformation is achieved through the upper-lower-bound approach:

$$f_i^{norm}(\vec{X}) = \frac{f_i(\vec{X}) - f_i^{min}}{f_i^{max} - f_i^{min}} \quad (85)$$

This approach does not face numerical issues, in cases where the denominator is 0 and receives values between 0 and 1 [65-66].

The decision variable vector for the conventional supercritical cycle is:

$$\vec{X} = \left[T_{evap}, p_{high}, \Delta T_{pp,evap}, \Delta T_{pp,cond}\right]^T \quad (86)$$

while for the recuperative cycle it is:

$$\vec{X} = \left[T_{evap}, p_{high}, \Delta T_{pp,evap}, \Delta T_{pp,cond}, \Delta T_{pp,rec}\right]^T \quad (87)$$

Table 4. Examined range of the decision variables for the supercritical conditions

T_{evap} = [(T_cr+1), 275] °C
p_{high} = [3.7,4.0] *MPa*
$\Delta T_{pp,evap}$ = [3,25] °C
$\Delta T_{pp,cond}$ = [3,25] °C
$\Delta T_{pp,rec}$ = [3,10] °C

Table 5. Weight coefficients for the multi-objective function

w_1 = 0.4
w_2 = 0.3
w_3 = -0.3

Table 6. Working conditions

Parameter	Value
condensation temperature	T_{cond} = 60 °C
evaporation pressure	$p_{high} \leq 4$ *MPa*
pressure ratio	$\pi \leq 30$
thermal oil inlet temperature	$T_{o,in}$ = 300 °C
thermal oil pressure	p_o = 2 *bar*
water inlet temperature	$T_{w,in}$ = 20 °C
water pressure	p_w = 2 bar
output power	W_{out} = 50 kW_{el}
expander isentropic efficiency	$n_{is,e}$ = 0.80
pump isentropic efficiency	$n_{is,p}$ = 0.80
electromechanical efficiency of expander-generator coupling	n_{em} = 0.90
biomass boiler efficiency	n_b=0.95
biomass lower heating value	*LHV* =16 *MJ/kg*

Table 7. Working fluid selection criteria

Criterion	Value
working fluid type	dry or isentropic
critical temperature	$T_{cr} > 100$ °C
ODP	$ODP \leq 0.05$
GWP	$GWP \leq 1000$
normal boiling point	$NBP \leq 60$ °C
triple point	$T_{cr} < 0$ °C
auto-ignition temperature	$T_{ign} > 300$ °C

Tables 4 and 5 summarize the examined ranges of the decision variables for the subcritical and the supercritical conditions respectively.

The weight coefficients for the objectives f_1,f_2 and f_3 receive the arbitrary values of 0.4, 0.3 and -0.3 respectively.

Working Conditions

The working conditions are presented in Table 6. The power output of the system is set at 50 kW_{el}. The expander machine is assumed to be a radial turbine with maximum working temperature of 275 °C and a constant isentropic efficiency of 0.80. The maximum working pressure is assumed 4 *MPa* and the maximum pressure ratio 30. The pump has also a constant isentropic efficiency of 0.80. The thermal oil enters the evaporator at temperature of 300 °C, while the water has an entry temperature of 20 °C. Both have a pressure of 2 *MPa*. The biomass fuel is assumed to have an average LHV of 16 *MJ/kg* [67]. Table contains the working conditions for both cycles.

It should be noted that, the properties of a fluid undergo rapid changes during phase change or supercritical flow. Therefore, the surface calculation must be divided into subsections. The total surface is the sum of these subsections [88-90]. It was found that the discretization into 100 subsections suffices for a low relative error (below 0.1%).

Lastly, the working fluids are selected using the constraints of Table 7 and their basic properties are depicted on Table 8. Their thermodynamic properties are calculated with CoolProp with NBP reference state (h = 0 *kJ/kg*, s = 0 *kJ/kgK*) for saturated liquid under pressure of 1 *atm*) [68-70]. As thermal oil Dowtherm Q was selected.

RESULTS AND DISCUSSION

The optimal solutions for the basic and recuperative cycle are depicted in Fig. 7 and 9 and Tables 9 and 11. The corresponding values of the examined parameters can be found in Figures 11-16 and Tables 10 and 12. Fig. 8 and 10 provide the average and best fitness values versus the generations.

Considering that the maximum pinch point temperature difference is 25 °C, it can be deduced that the maximum

Table 8. Properties of the selected working fluids by order of increasing critical temperature [68-70]

Working fluid	Chemical formula	Chemical class	Cas number	Fluid type	T_{cr} [°C]	p_{cr} [MPa]	NBP [°C]	T_{tr} [°C]	T_{ign} [°C]	ODP [-]	GWP [-]
R124	C_2HClF_4	Hydrochlorofluoro-carbons (HCFC)	2837-89-0	isen	122.28	3.62	-11.96	-153.15	-	0.02	527
IsoButane	$(CH_3)_2CHCH_3$ or C_4H_{10}	Alkanes	75-28-5	dry	134.67	3.63	-11.75	-159.42	460.00	0	20
R245fa	$C_3H_3F_5$	Hydrofluoro-carbons (HFC)	460-73-1	dry	153.86	3.65	15.05	-102.10	-	0	882
Isopentane	C_5H_{12} or $(CH_3)_2$-CH-CH_2-CH_3	Alkanes	78-78-4	dry	187.20	3.38	27.83	-160.50	420.00	0	4
Cyclopentane	C_5H_{10}	Cycloalkanes	287-92-3	dry	238.57	4.57	49.26	-93.45	320.00	0	0
Water	H_2O	Inorganics	7732-18-5	wet	373.95	22.06	100.00	0.01	-	0	0
Dowtherm Q	$C_{22}H_{24}$	Mixture of diphenylethane and alkylated aromatics	511256-19-2	-	489.00	2.4	N/A	N/A	412.00	0	0

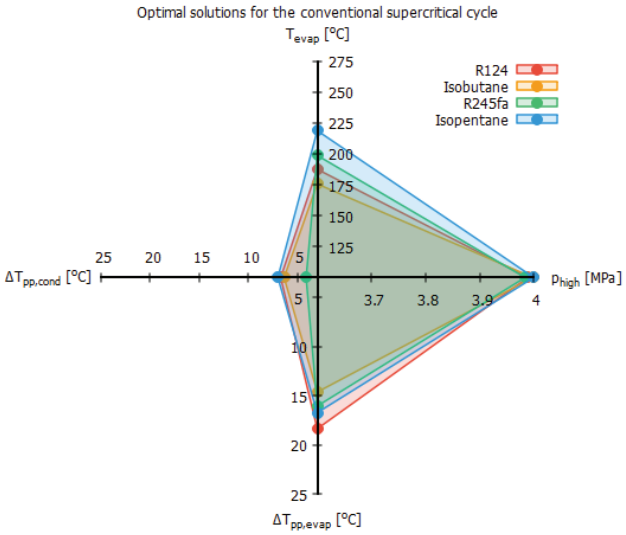

Figure 7. Optimal solutions for the conventional supercritical cycle.

operating temperature cannot exceed 275 °C. The evaporation temperatures of the recuperative cycle are located near that boundary. In contrast, in the case of conventional cycle an important deviation from the maximum allowed temperature is noticed. Furthermore, it is observed that the optimal evaporation pressure is located near the maximum allowed value of 4 *MPa* for all working fluids, regardless of the cycle type.

The pinch point temperature difference receives low values for the condenser and the recuperator. In the first case the value range is 4 - 7 °C, while in the latter it is 4 - 6 °C. The corresponding values for the evaporator are remarkably higher. Generally, the lowest temperature difference is higher than 15 °C, with one exception. For R245fa in the recuperative cycle this value is below 10 °C.

Fitness diagrams show that isopentane generally performs better, with R245, isobutane and R124 following.

R124 and isobutane display the lowest values of thermal efficiency, with 0.0985 and 0.1072 respectively. R245fa

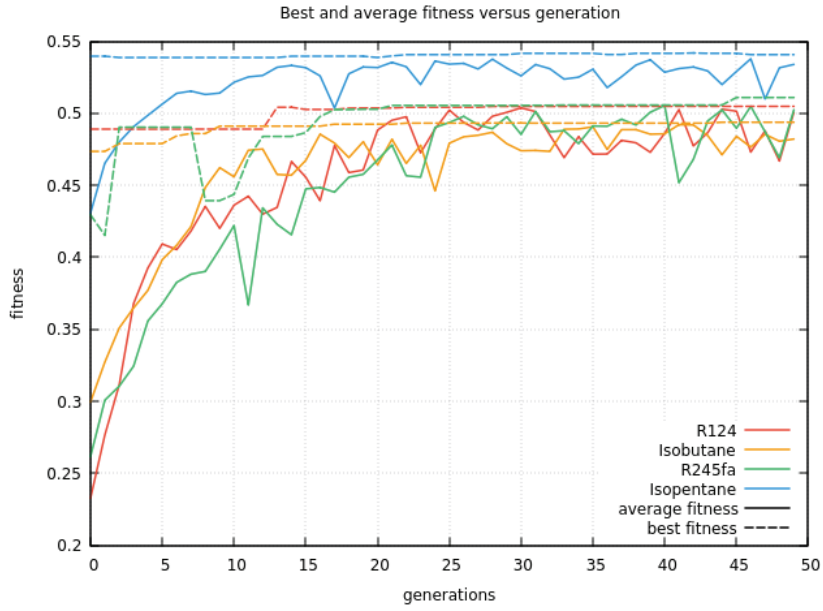

Figure 8. Average and best fitness versus generations for the conventional supercritical cycle.

Table 9. Optimal solutions for the conventional supercritical cycle

Working fluid	T_{evap} [°C]	p_{high} [°C]	$\Delta T_{pp,evap}$ [°C]	$\Delta T_{pp,cond}$ [°C]
R124	187.4900	3.9890	18.3483	6.7139
Isobutane	175.5892	3.9982	14.6251	6.3584
R245fa	198.6879	3.9836	16.0459	4.1194
Isopentane	218.6338	4.0000	16.7134	7.0019

Table 10. Parameter values corresponding to the optimal solution for the conventional supercritical cycle

Working fluid	R124	Isobutane	R245fa	Isopentane
n_{th} [-]	0.0985	0.1072	0.1258	0.1442
n_{ex} [-]	0.8176	0.8210	0.8418	0.8547
w_{net} [kJ/kg]	21.4507	50.3437	35.5128	81.8093
$\dot{m}_{wf}$ [kg/s]	2.5899	1.1035	1.5644	0.6791
$\dot{m}_{bm}$ [kg/s]	0.0371	0.0341	0.0290	0.0253
$n_{el,chp}$ [-]	0.0842	0.0917	0.1076	0.1233
$n_{th,chp}$ [-]	0.8564	0.8481	0.8305	0.8130
n_{chp} [-]	0.9406	0.9398	0.9380	0.9363
PHR [-]	0.0984	0.1081	0.1295	0.1516
PESR [-]	0.1714	0.1805	0.1992	0.2169
A_{evap} [m^2]	1.6927	1.6685	1.8349	1.9932
A_{cond} [m^2]	2.1707	2.0198	2.0161	1.4476
$T_{o,out}$ [°C]	79.6504	77.3261	76.6785	79.2119
m_o [kg/s]	1.1750	1.0700	0.9098	0.8015
$T_{w,out}$ [°C]	74.2279	69.5821	72.9672	71.7542
$\dot{m}_w$ [kg/s]	2.2423	2.2317	1.7435	1.5242

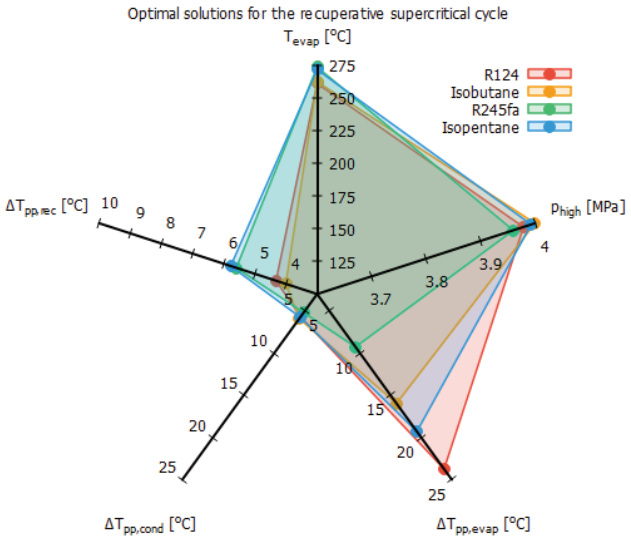

Figure 9. Optimal solutions for the recuperative supercritical cycle.

follows with 0.1258. The maximum achieved value of 0.1442 corresponds to isopentane. Internal recuperation is beneficial to the thermal efficiency. The percentage increase can surpass 80%. Even though isopentane shows the smallest gain, it achieves the highest n_{th}, 0.2328.

The values of exergy efficiency are higher than 0.80 for all working fluids. The highest value of 0.8547 is exhibited by isopentane. The use of recuperation improves slightly n_{ex} (below 1%). With internal preheating the required exergetic input is reduced in a manner, that practically counterbalances the improvement in terms of rate of exergy destruction.

In the conventional cycle, the lowest total exchanger surface is 3.4407m^2 and is attributed to isopentane. Isobutane, R245fa and R124 follow with 3.6883^2, 3.8510^2 and 3.8634^2 respectively.

The presence of an internal heat exchanger leads to an increase of A_t. Isobutane and isopentane require 12.74% and 12.55% more surface respectively. R124 requires 5.00% and R245fa 0.6117% more surface.

Figure 10. Average and best fitness versus generations for the recuperative supercritical cycle.

Table 11. Optimal solutions for the recuperative supercritical cycle

Working fluid	T_{evap} [°C]	p_{high} [°C]	$\Delta T_{pp,evap}$ [°C]	$\Delta T_{pp,cond}$ [°C]	$\Delta T_{pp,rec}$ [°C]
R124	260.7196	3.9787	23.7430	5.6816	4.3179
Isobutane	262.0709	3.9998	15.9703	5.9073	4.0050
R245fa	273.3199	3.9600	9.2658	5.1888	5.5927
Isopentane	271.2223	3.9931	19.2970	5.7418	5.7728

In terms of specific net work and working fluid mass flow rate, isopentane displays superior performance. In the conventional cycle the values of 81.8093 *kJ/kg* and 0.6791 *kg/s* are achieved. A noteworthy gain results from the use of a recuperator. The improvement for w_{net} is 25 - 45%, while for $\dot{m}_{wf}$ it is 20 - 30% across all fluids. Thusly, isopentane reaches specific net work 103.3 *kJ/kg* and required mass flow rate 0.5378 *kg/s*. The large deviation is attributed to the fact that the optinal evaporation temperature between the two cycles differs greatly.

R245fa and isopentane exhibit the highest values for the PHR and PESR indices. In the case of the conventional cycle, R245fa achieves 0.1295 for PHR and 0.1992 for PESR. Internal recuperation improves these values to 0.2390 and 0.2742 respectively. Similarly, for isopentane PHR is 0.1516 without recuperation and 0.28 with recuperation. The presence of a recuperator improves PESR from 0.2169 to 0.2957.

The overall cogeneration efficiency receives value in the region 0.92 - 0.95, without noticeable differences between cycles and working fluids. In the conventional cycle R124 displays at the same time the maximum thermal and minimum electrical cogeneration efficiency. In contrast, isopentane achieves the maximum electrical and the minimum thermal cogeneration efficiency. The addition of an internal heat exchanger leads to noticeable improvements. For instance, in the case of isopentane $n_{el,chp}$ increased from 0.1235 to 0.2029 and $n_{th,chp}$ from 0.7246 to 0.8130.

The required biomass mass flow rate in the conventional cycle lies in the range 0.02 - 0.04 *kg/s*, with isopentane and R124 exhibiting the minimum and maximum values respectively. Biomass fuel consumption can be reduced greatly through internal preheating. The reduction can be more than 45% (R124 and isobutane).

Table 12. Parameter values corresponding to the optimal solution for the recuperative supercritical cycle

Working fluid	R124	Isobutane	R245fa	Isopentane
n_{th} [-]	0.1792	0.1960	0.2098	0.2373
n_{ex} [-]	0.8213	0.8333	0.8440	0.8555
w_{net} [*kJ/kg*]	28.3727	72.9872	47.0299	103.3000
$\dot{m}_{wf}$ [*kg/s*]	1.9581	0.7612	1.1813	0.5378
$\dot{m}_{bm}$ [*kg/s*]	0.0204	0.0186	0.0174	0.0154
$n_{el,chp}$ [-]	0.1532	0.1676	0.1794	0.2029
$n_{th,chp}$ [-]	0.7798	0.7638	0.7507	0.7246
n_{chp} [-]	0.9330	0.9314	0.9301	0.9275
PHR [-]	0.1965	0.2194	0.2390	0.2800
PESR [-]	0.2485	0.2628	0.2742	0.2957
A_{evap} [m^2]	1.2967	1.4491	1.4502	1.3131
A_{cond} [m^2]	1.2789	1.1068	1.0781	0.9249
A_{rec} [m^2]	1.4811	1.6025	1.3462	1.6347
$T_{o,out}$ [°C]	156.7209	160.8447	165.3161	189.3969
m_o [*kg/s*]	0.9439	0.8862	0.8527	0.9043
$T_{w,out}$ [°C]	56.5785	55.9297	56.6073	56.3796
$\dot{m}_w$ [*kg/s*]	1.6649	1.5180	1.3675	1.7445

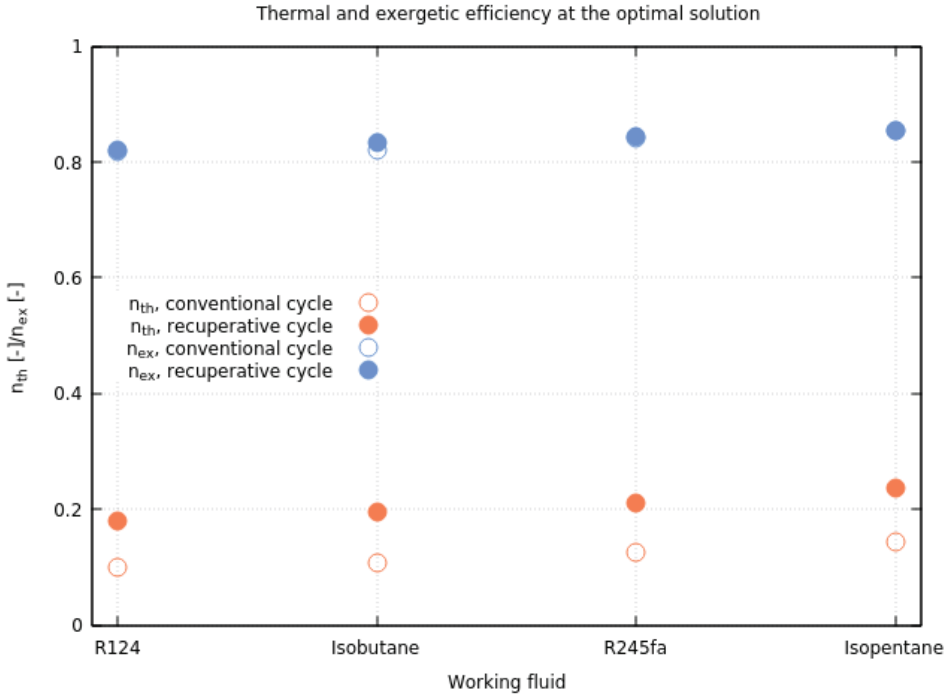

Figure 11. Thermal and exergetic efficiency corresponding to the optimal solution for the supercritical cycle.

The lowest thermal oil exit temperature is 76.6785 °*C* in the basic cycle and 156.7209 °*C* in the recuperative cycle with R124. The lowest thermal oil mass flow rate is 0.8015 *kg/s* for isopentane without recuperation. R245fa with recuperation achieves 0.8527 *kg/s*.

In the conventional cycle, the maximum water exit temperature is 74.2279 °*C* and is achieved by R124, while the lowest water mass flow rate is 1.5242 *kg/s* and is attributed to isopentane. In the recuperative cycle, R245fa achieves exit temperature 56.6073 °*C* and mass flow rate 1.3675 *kg/s*. Generally, the use of recuperation lowers $T_{w,out}$ significantly, by 15-20 °*C*.

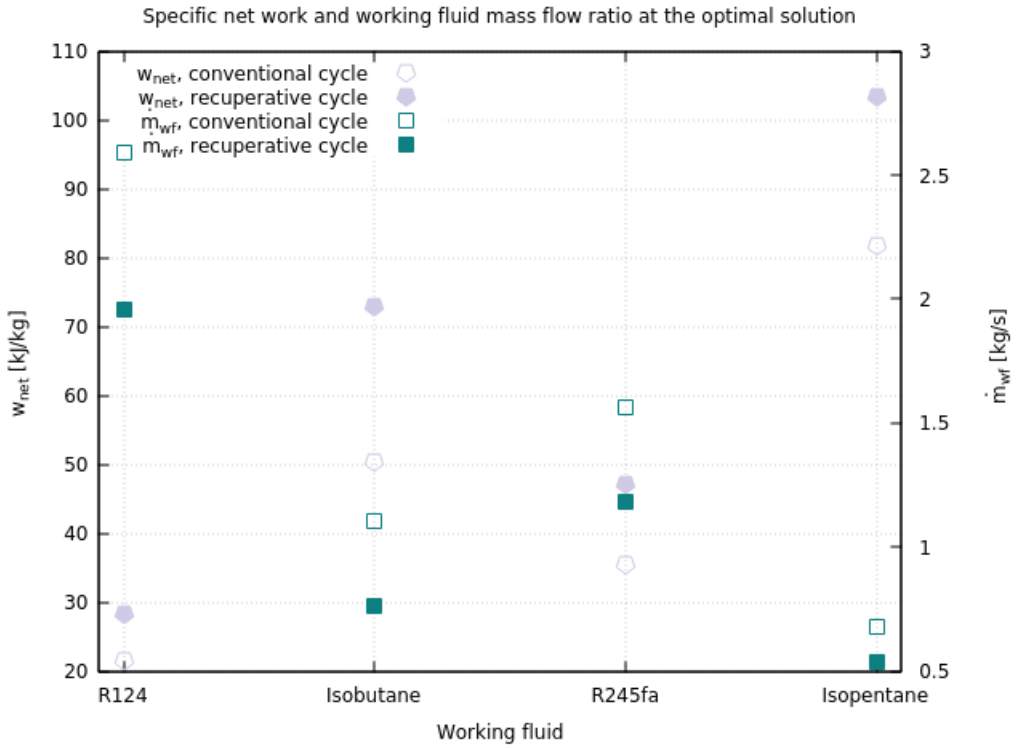

Figure 12. Specific net work and working fluid mass flow rate corresponding to the optimal solution for the supercritical cycle.

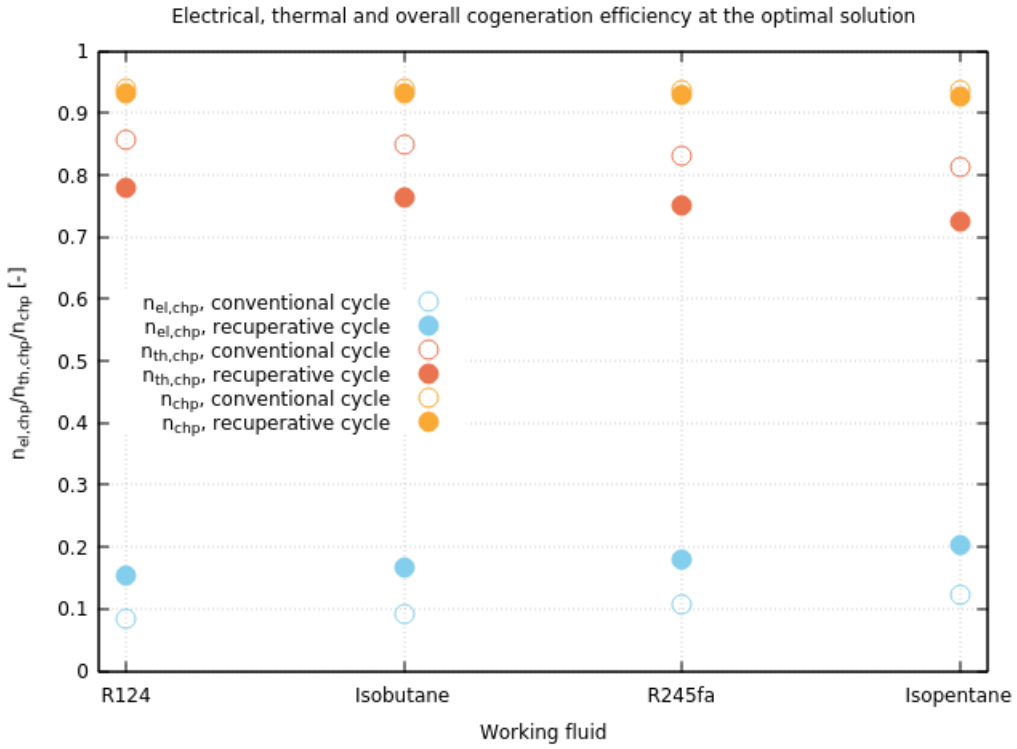

Figure 13. Electrical, thermal and overall cogeneration efficiency corresponding to the optimal solution for the supercritical cycle.

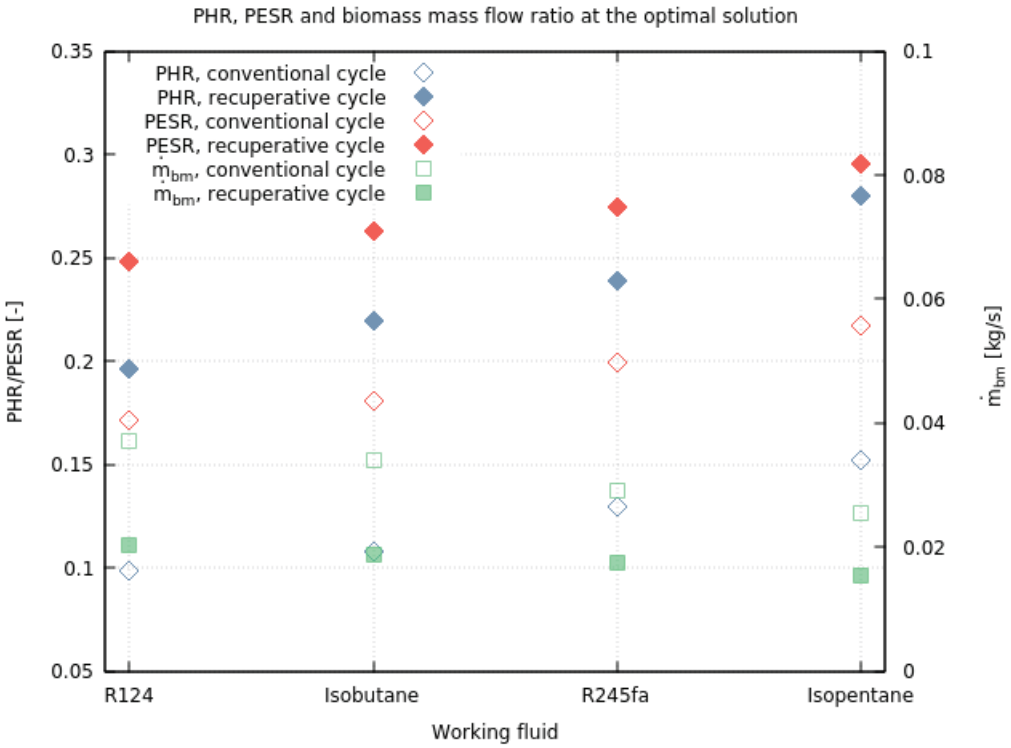

Figure 14. PHR, PESR indices and biomass mass flow rate corresponding to the optimal solution for the supercritical cycle.

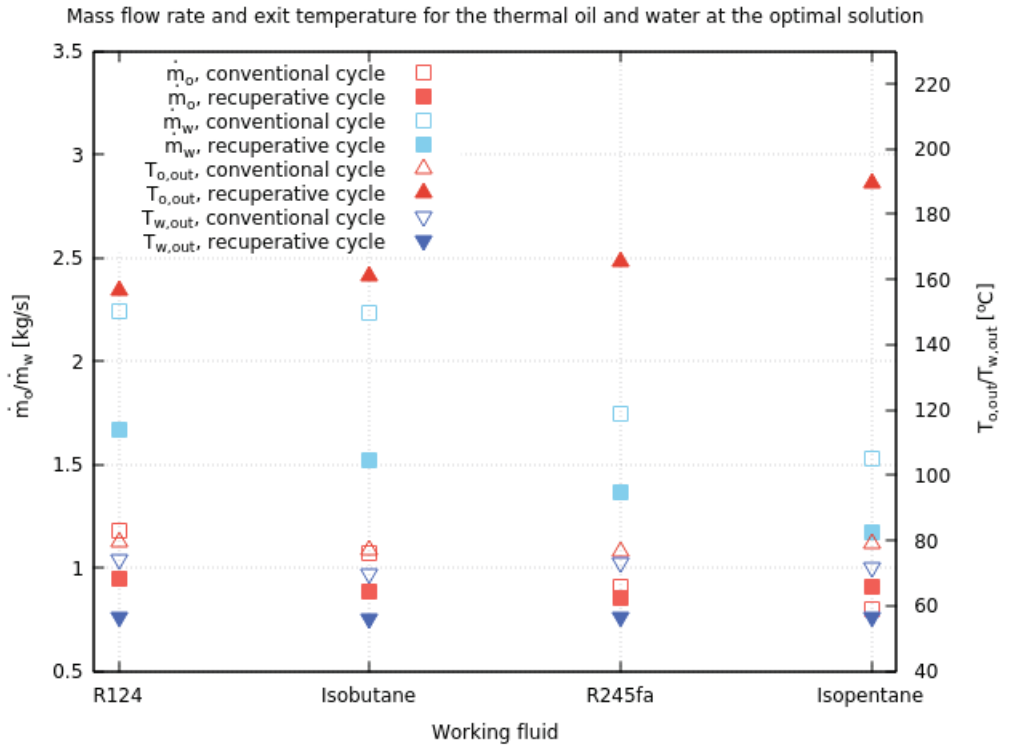

Figure 15. Mass flow rate and exit temperature for the thermal oil and water corresponding to the optimal solution for the supercritical cycle.

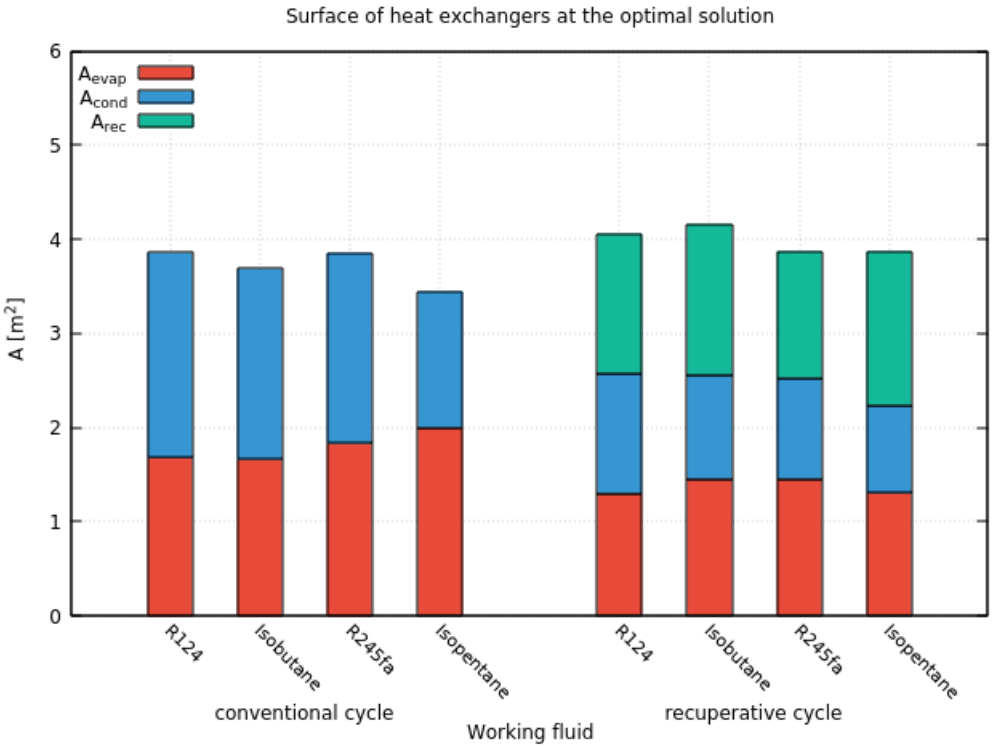

Figure 16. Heat exchanger surface histogram corresponding to the optimal solution for the supercritical cycle.

CONCLUSIONS

In the present paper, a steady-state thermodynamic model for a 50 kW_{el} biomass CHP-ORC was developed and four candidate fluids were selected: R124, isobutane, R245fa and isopentane. The genetic algorithm was used for the optimization of the system under supercritical conditions. The fitness function was a linear combination of the thermal efficiency, the exergy efficiency and the total heat exchanger surface. The evaporation temperature and pressure and the pinch point temperature differences at the heat exchangers were selected as decision variables.

The comparison of the results revealed a series of interesting observations. Firstly, there is no single working fluid that is superior in every aspect. However, isopentane stands out. It has also been noted that, working fluids with higher critical temperature display higher thermal efficiency. The use of an internal heat exchanger leads to an increase in total surface, despite the reduction in evaporator and condenser surface. In addition, a recuperator restricts the water exit temperature at lower levels. Therefore, its use is advisable only when the increase in thermal efficiency offsets the increase in cost and the water exit temperature can be maintained at sufficient levels. Lastly, it is evident that, optimization alone is not enough. The system designer must make the final decision based on subjective criteria.

Another two noteworthy observations are related to the optimal values of the decision variables. The optimal pinch point temperature difference at the recuperator tends towards the lower values 4 - 6 °*C*. In addition, the evaporation temperature of the supercritical cycle receives values in the region 3.95 - 4 *MPa*, for all working fluids, for both conventional and recuperative cycle. These observations can be exploited, in order to reduce the search space and lead to a faster convergence of the genetic algorithm. No systematic tendencies were observed for the remaining decision variables.

An important aspect of the CHP-ORC system is the utilization of the heat, which the condenser would otherwise reject. In this case, the total cogeneration efficiency surpasses 90%, while simultaneously saving 20 - 30% biomass fuel.

The paper concludes with suggestions for future research. The evaporator is significant source of exergy destruction. During the phase change, the temperature of a pure substance remains constant, which leads to an increased temperature difference between the two streams. This is tantamount to an increased rate of exergy destruction. One of the most effective ways to mitigate the evaporator losses is the use of zeotropic mixtures. Their main attribute is the non-isothermal phase change. Compared to pure substances, zeotropic mixtures have not been investigated at the same degree.

The heat transfer on the interior of plate heat exchanger is a complex phenomenon. It depends on the characteristics of the flow, the geometry of the plates and the configuration

of the flow. Consequently there is no general theory or correlation, which describes all possible flow conditions and combinations of geometric parameters. The calculation of the Nusselt number relies on semi-empirical correlations, that are developed for specific heat exchangers, geometries and flow regiments. Unlike the single-phase region, the evaporation, condensation and supercritical flow have not been investigated sufficiently. Also, apart from the chevron angel, the influence of the other geometric parameters on the heat transfer characteristics has yet to be delineated.

The success and efficiency of the genetic algorithm is greatly affected by its control parameters. The dynamic adjustment variables such as the crossover and mutation probability could offer faster convergence. This area has plenty of room for research activity. A relative attempt has been performed by A. Hassanat et al [64].

Lastly, the relationship between critical temperature and thermal efficiency has been verified before by J. Xu and C. Yu [8]. Working fluids with higher critical temperature are expected to exhibit higher values of n_{th}. This conclusion could be expanded to more parameters. A similar tendency is observed for other indicators such as the thermal and electrical cogeneration efficiencies ($n_{el,chp}$, $n_{th,chp}$) and the PHR and PESR ratios. This requires further systematic investigation with more fluids, in order to verify it.

ACKNOWLEDGEMENTS

The present work was financially supported by National Technical University's Research Committee scholarship.

NOMENCLATURE

Latin characters

A_{ch}	$[m^2]$	channel surface
A_e	$[m^2]$	plate effective surface
A_p	$[m^2]$	plate projected surface
b	$[m]$	mean channel spacing
c	$[J/kgK]$	specific heat capacity
C	$[J/sK]$	heat capacity rate
D_h	$[m]$	hydraulic diameter
D_p	$[m]$	port diameter
E	$[J]$	energy
$\dot{E}_x$	$[W]$	exergy rate
$\dot{E}_{xd}$	$[W]$	exergy destruction rate
f	[-]	objective function
G	$[kg/sm^2]$	mass velocity
$F(X)$	[-]	multi-objective function
Ge	[-]	geometric parameter
h	$[J/kg]$	specific enthalpy
k	$[W/mK]$	thermal conductivity
L_c	$[m]$	compressed PHE length
L_e	$[m]$	effective plate length
L_p	$[m]$	vertical distance between ports
LHV	$[MJ/Nm^3]$	lower heating value
$\dot{m}$	$[kg/s]$	mass flow rate
n	[-]	efficiency
n_{chr}	[-]	number of chromosomes
n_{gen}	[-]	number of genes
n_{gener}	[-]	number of generations
n_{par}	[-]	number of parents
N_{cp}	[-]	number of channels per pass
N_e	[-]	number of effective plates
N_p	[-]	number of passes
N_t	[-]	total number of plates
Nu	[-]	Nusselt number
p	$[Pa\ or\ atm]$	pressure
p	$[m]$	plate pitch
p_c	[-]	crossover probability
p_m	[-]	mutation probability
P	$[m]$	perimeter
$PESR$	[-]	primary energy saving ratio
PHR	[-]	power-to-heat ratio
Pr	[-]	Prandtl number
q	$[J/kg]$	specific heat energy
$\dot{q}$	$[W/m^2]$	heat flux
$\dot{Q}$	$[W]$	heat transfer rate
Re	[-]	Reynolds number
s	$[J/kgK]$	specific entropy
t	$[m]$	corrugation thickness
T	$[K\ or\ °C\ ]$	temperature
U	$[W/m^2\ K]$	overall heat transfer coefficient
V	$[m^2/s]$	velocity
w	$[J/kg]$	specific work
w	[-]	weight factor
$\dot{W}$	$[W]$	power
W_e	$[m]$	effective plate width
W_p	$[m]$	horizontal distance between plate ports
X	[-]	plate dimensionless parameter

Greek characters

a	$[W/m^2\ K]$	convection coefficient
β	[°]	chevron angle
Δ	$[J/kg]$	difference
λ	$[m]$	corrugation pitch or wavelength
μ	$[kg/ms]$	dynamic viscosity
v	$[m^2/s]$	kinematic viscosity

π	[-]	pressure ratio
ρ	$[kg/m^3]$	density
σ	$[N/m]$	surface tension
Φ	[-]	enhancement factor

Indices

0	dead state
bm	biomass
boiler	boiler
c	cold stream
ch	channel
chp	cogeneration
cond	condenser
cr	critical
d	destruction
e	expander
eq	equivalent
el	electric
em	electromechanical
evap	evaporator or evaporating section
f	saturated liquid state
fg	liquid-vapor two-phase region
g	saturated vapor state
h	hot stream
ign	auto-ignition
in	input
is	isentropic
lm	logarithmic
m	mean of bulk
max	maximum
min	minimum
net	net
norm	normalized
o	thermal oil
orc	ORC
out	output
p	pump
pl	plate
preheat	preheating section
pp	pinch point
ps	pseudocritical
r	recuperative
ref	reference
rec	recuperator
s	saturation
sub	subcritical section
super	supercritical section
superheat	superheating section
t	total
tr	triple
v	vertical
w	cooling water
wf	working fluid
wl	wall

Abbreviations

Latin characters

CAS	Chemical Abstracts Service
CHP	Combined Heat and Power
GA	Genetic Algorithm
GWP	Global Warming Potential
IHE	Internal Heat Exchanger
LHV	Lower Heating Value
MOO	Multi-Objective Optimization
NBP	Normal Boiling Point
ODP	Ozone Depletion Potential
ORC	Organic Rankine Cycle
PHE	Plate Heat Exchanger
SOO	Single-Objective Optimization
WHR	Waste Heat Recovery

ORC states

Point	***Description***	***Working fluid state***
1	Condenser exit	Saturated liquid
2_{is}	Pump exit, isentropic compression	Compressed liquid
2	Pump exit, real compression	Compressed liquid
2_r	Recuperator, cold stream exit	Compressed liquid
2_f	Evaporator	Saturated liquid
3_g	Evaporator	Saturated vapor
3	Evaporator exit	Saturated vapor, superheated Vapor or supercritical state
4_{is}	Turbine exit, isentropic expansion	Superheated vapor
4	Turbine exit, real expansion	Superheated vapor
4_r	Recuperator, hot stream exit	Superheated vapor
4_g	Evaporator	Saturated vapor

AUTHORSHIP CONTRIBUTIONS

Authors equally contributed to this work.

DATA AVAILABILITY STATEMENT

The authors confirm that the data that supports the findings of this study are available within the article. Raw data that support the finding of this study are available from the corresponding author, upon reasonable request.

CONFLICT OF INTEREST

The author declared no potential conflicts of interest with respect to the research, authorship, and/or publication of this article.

ETHICS

There are no ethical issues with the publication of this manuscript.

REFERENCES

[1] Schuster A, Karellas S, Kakaras E, Spliethoff H. Energetic and economic investigation of Organic Rankine Cycle applications. Appl Thermal Eng 2009;29:1809−1817. [CrossRef]

[2] Lolos PA, Rogdakis ED. A Kalina power cycle driven by renewable energy sources. Energy 2009;34:457−464. [CrossRef]

[3] Upadhyaya S, Gumtapure V. Parametric investigation of open-drive scroll expander for micro Organic Rankine Cycle applications. J Thermal Eng 2021;7:1110−11120. [CrossRef]

[4] Quoilin S, Van Den Broek M, Declaye S, Dewallef P, Lemort V. Techno-economic survey of Organic Rankine Cycle (ORC) systems. Renew Sustain Energy Rev 2013;22:168−186. [CrossRef]

[5] Bao J, Zhao L. A review of working fluid and expander selections for organic rankine cycle. Renew Sustain Energy Rev 2013;24:325−342. [CrossRef]

[6] Reddy PK, Bhagyashekar MS. Experimental testing of scroll machine driven by compressed air for power generation and its integration in small scale organic Rankine Cycle. J Thermal Eng 2021;7:1457−1467. [CrossRef]

[7] Ozdemir E, Kilic M. Thermodynamic analysis of basic and regenerative Organic Rankine Cycles using dry fluids from water heat recovery. J Thermal Eng 2018;4:2381−2393. [CrossRef]

[8] Xu J, Yu C. Critical temperature criterion for selection of working fluids for subcritical pressure Organic Rankine Cycles. Energy 2014;74:719−733. [CrossRef]

[9] Jankowski M, Borsukiewicz A. Multi-objective approach for determination of optimal operating parameters in low-temperature ORC power plant. Energy Convers Manag 2019;200:112075. [CrossRef]

[10] Mohammadi H, Mohammadi M. Optimization of the micro combined heat and power systems considering objective functions, components and operation strategies by an integrated approach. Energy Convers Manag 2020;208:112610. [CrossRef]

[11] Konak A, Coit DW, Smith AE. Multi-objective optimization using genetic algorithms: A tutorial. Reliab Eng Syst Saf 2006;91:992−1007. [CrossRef]

[12] Rahbar K, Mahmoud S, AL-Dadah RK, Moazami N. Parametric analysis and optimization of a small-scale radial turbine for Organic Rankine Cycle. Energy 2015;83:696−711. [CrossRef]

[13] Imran M, Park BS, Kim HJ, Lee DH, Usman M, Heo M. Thermo-economic optimization of Regenerative Organic Rankine Cycle for waste heat recovery applications. Energy Convers Manag 2014;87:107−118. [CrossRef]

[14] Wei D, Lu X, Lu Z, Gu J. Performance analysis and optimization of Organic Rankine Cycle (ORC) for waste heat recovery. Energy Convers Manag 2007;48:1113−1119. [CrossRef]

[15] Jankowski M, Borsukiewicz A, Szopik-Depczyńska K, Ioppolo G. Determination of an optimal pinch point temperature difference interval in ORC power plant using multi-objective approach. J Clean Prod 2019;217:798−807. [CrossRef]

[16] Sani MM, Noorpoor A, Motlagh MS. Multi-objective optimization of waster heat recovery in cement industry (a case study). J Therm Eng 2020;6:604−618. [CrossRef]

[17] Bademlioglu AH, Canbolat AS, Kaynakli O. Multi-objective optimization of parameters affecting Organic Rankine Cycle performance characteristics with Taguchi-Grey relational analysis. Renew Sustain Energy Rev 2020;117:109483. [CrossRef]

[18] Choi HW, Na S-I, Hong SB, Chung Y, Kim DK, Kim MS. Optimal design of Organic Rankine Cycle recovering LNG cold energy with finite heat exchanger size. Energy 2021;217:119268. [CrossRef]

[19] Wang D, Ma Y, Tian R, Duan J, Hu B, Shi L. Thermodynamic evaluation of an ORC system with a low pressure saturated steam heat source. Energy 2018;149:375−385. [CrossRef]

[20] Karellas S, Schuster A. Supercritical fluid parameters in organic rankine cycle applications. Int J Thermodyn 2008;11:101−108.

[21] Qiu G. Selection of working fluids for micro-CHP systems with ORC. Renew Energy 2012;48:565−570. [CrossRef]

[22] Drescher U, Bruggemann D. Fluid selection for the Organic Rankine Cycle (ORC) in biomass power and heat plants. Appl Therm Eng 2007;27:223−228. [CrossRef]

[23] Akkaya AV. Performance analyzing of an Organic Rankine Cycle under different ambient conditions. J Therm Eng 2017;3:1498−1504. [CrossRef]

[24] Moran MJ, Shapiro HN. Fundamentals of engineering thermodynamics. 5th ed. John Wiley & Sons; 2006.
[25] Desai NB, Bandyopadhyay S. Process integration of Organic Rankine Cycle. Energy 2009;34:1674−1686. [CrossRef]
[26] Jumel S, Le-Van L, Feidt M, Kheiri A. Working fluid selection and performance comparison of subcritical and supercritical Organic Rankine Cycle (ORC) for low-temperature waste heat recovery. ECEEE 2012 Summer Study on Energy Efficiency in Industry.
[27] Tchanche BF, Tchanche BF, Lambrinos G, Frangoudakis A, Papadakis G. Low-grade heat conversion into power using organic Rankine cycles - A review of various applications. Renew Sustain Energy Rev 2011;15:3963−3979. [CrossRef]
[28] Liu X, Zhang Y, Shen J. System performance optimization of ORC-based geo-plant with R245fa under different geothermal water inlet temperatures. Geothermics 2017;66:134−142. [CrossRef]
[29] Wang R, Jiang L, Ma Z, Gonzalez-Diaz A, Wang Y, Roskilly AP. Comparative analysis of small-scale organic rankine cycle systems for solar energy utilisation. Energies 2019;12:829. [CrossRef]
[30] Mudasar R, Aziz F, Kim MH. Thermodynamic analysis of Organic Rankine Cycle used for flue gases from biogas combustion. Energy Convers Manag 2017;153:627−640. [CrossRef]
[31] Chen Q, Xu J, Chen H. A new design method for organic rankine cycles with constraint of inlet and outlet heat carrier fluid temperatures coupling with the heat source. Appl Energy 2012;98:562−573. [CrossRef]
[32] Incropera F, Incropera FP, DeWitt DP, Bergman TL. Fundamentals of heat and mass transfer. 6th ed. New York: John Wiley & Sons; 2007.
[33] Wang J, Diao M, Yue K. Optimization on pinch point temperature difference of ORC system based on AHP-Entropy method. Energy 2017;141:97−107. [CrossRef]
[34] Han Z, Li P, Han X, Mei Z, Wang Z. Thermo-economic Performance analysis of a regenerative superheating Organic Rankine Cycle for waste heat recovery. Energies 2017;10:1593. [CrossRef]
[35] Oyewunmi OA, Kirmse C, Markides CN. Performance of working-fluid mixtures in ORC-CHP systems for different heat-demand segments and heat-recovery temperature levels. Energy Convers Manag 2017;148:1508−1524. [CrossRef]
[36] Shu G, Liu L, Tian H, Wei H, Yu G. Parametric and working fluid analysis of a dual-loop Organic Rankine Cycle (DORC) used in engine waste heat recovery. Appl Energy 2014;113:1188−1198. [CrossRef]
[37] Kang Z, Zhu J, Lu X, Li T, Wu X. Parametric optimization and performance analysis of zeotropic mixtures for an Organic Rankine Cycle driven by low-medium temperature geothermal fluids. Appl Therm Eng 2015;89:323−339. [CrossRef]
[38] Official Journal of the European Parliament. Directive 2004/8EC of the European Parliament and of the Council of 11 February 2004 on the promotion of cogeneration based on a useful heat demand in the internal energy market and amending Directive 92/42/EEC.
[39] Kanoglu M, Dincer I. Performance assessment of cogeneration plants. Energy Convers Manag 2009;50:76−81. [CrossRef]
[40] Nesheim SJ, Ertesvag IS. Efficiencies and indicators defined to promote Combined Heat and Power. Energy Convers Manag 2007;48:1004−1015. [CrossRef]
[41] Qiu G, Shao Y, Li J, Liu H, Riffat SB. Experimental investigation of a biomass-fired ORC-based micro-CHP for domestic applications. Fuel 2012;96:374−382. [CrossRef]
[42] Zhu Y, Li W, Li J, Li H, Wang Y, Li S. Thermodynamic analysis and economic assessment of biomass-fired Organic Rankine Cycle Combined Heat and Power system integrated with CO2 capture. Energy Convers Manag 2020;204:112310. [CrossRef]
[43] Sarkar J. Generalized pinch point design method of subcritical-supercritical Organic Rankine Cycle for maximum heat recovery. Energy 2018;143:141−150. [CrossRef]
[44] Kim KH, Ko HJ, Kim K. Assessment of pinch point characteristics in heat exchangers and condensers of ammonia-water based power cycles. Appl Energy 2014;113:970−981. [CrossRef]
[45] Khan TS, Khan MS, Chyu M-C, Ayub ZH. Experimental investigation of evaporation heat transfer and pressure drop of ammonia in a 60° chevron plate heat exchanger. Int J Refrig 2012;35:336−348. [CrossRef]
[46] Thulukkanam K. Heat exchanger design handbook. 2nd ed. Boca Raton, USA: CRC Press; 2013. [CrossRef]
[47] Kakac S, Liu H. Heat exchangers. Selection, rating and thermal design. 2nd edition. Boca Raton, USA: CRC Press; 2002.
[48] Dovic D, Palm B, Svaic S. Generalized correlations for predicting heat transfer and pressure drop in plate heat exchanger channels of arbitrary geometry. Int J Heat Mass Transf 2009;52:4533−4563. [CrossRef]
[49] Sagia A, Sagia Z. Heat Transfer I. National Technical University of Athens; 2018, Athens, Greece.
[50] Zhang J, Zhu X, Mondejar ME, Haglind F. A review of heat transfer enhancement techniques in plate heat exchangers. Renew Sustain Energy Rev 2019;101:305−328. [CrossRef]
[51] Ayub ZH. Plate heat exchanger literature survey and new heat transfer and pressure drop correlations for refrigerant evaporators. Heat Transf Eng 2003;24:3−16. [CrossRef]
[52] Garcia-Cascales JR, Vera-García F, Corberán-Salvador JM, Gonzálvez-Maciá J. Assessment of boiling and condensation heat transfer correlations

in the modelling of plate heat exchangers. Int J Refrig 2007;30:1029−1041. [CrossRef]
[53] Junqi D, Xianhui Z, Jianhang W. Experimental investigation on heat transfer characteristics of plat heat exchanger applied in Organic Rankine Cycle (ORC). Appl Therm Eng 2017;112:1137−1152. [CrossRef]
[54] Imran M, Pili R, Usman M, Haglind F. Dynamic modeling and control strategies of Organic Rankine Cycle systems: methods and challenges. Appl Energy 2020;115537. [CrossRef]
[55] Kim YS. An experimental study on evaporation heat transfer characteristics and pressure drop in plate heat exchanger. [Master thesis], Seoul, South Korea: Yonsei University; 1999.
[56] Forooghi P, Hooman K. Experimental analysis of heat transfer of supercritical fluids in plate heat exchangers. Int J Heat Mass Transf 2014;74:448−459. [CrossRef]
[57] Harmen, Adriansyah W, Abdurrachim, Darmawan Pasek A. Theoretical investigation of heat transfer correlations for supercritical organic fluids. AIP Conf Proceed 2018;1984:020011. [CrossRef]
[58] Karellas S, Schuster A, Leontaritis AD. Influence of supercritical ORC parameters on plate heat exchanger design. Appl Thermal Eng 2012;33-34:70−76. [CrossRef]
[59] Kruizenga A, Li H, Anderson M, Corradini M. Supercritical carbon dioxide heat transfer in horizontal semicircular channels. J Heat Transf 2012;134:081802. [CrossRef]
[60] Han DH, Lee KJ, Kim YH. The characteristics of condensation in brazed plate heat exchangers with different chevron angles. J Korean Phys Soc 2003;43:66−73.
[61] Buonopane RA, Troupe RA, Morgan JC. Heat transfer design method for plate heat exchangers. Chem Eng Prog 1963;59:57−61.
[62] Goldberg DE. Genetic Algorithms in Search, Optimization and Machine Learning. Boston, Massachusetts, USA: Addison-Wesley Publishing Company; 1989,
[63] Gen M, Cheng R. Genetic Algorithms and Engineering Design. West Sussex, England: John Wiley & Sons; 1997
[64] Hassanat A, Hassanat A, Almohammadi K, Almohammadi K, Alkafaween E, Abunawas E, Hammouri A, Surya Prasath VB. Choosing mutation and crossover ratios for genetic algorithms-A review with a new dynamic approach. Information 2019;10:390. [CrossRef]
[65] Marler RT, Arora JS. Function-transformation methods for multi-objective optimization. Eng Optimization 2005;36:551−570. [CrossRef]
[66] Konak A, Coit DW, Smith AE. Multi-objective optimization using genetic algorithms: A tutorial. Reliability Eng System Safety 2006;91:992−1007. [CrossRef]
[67] Telmo C, Lousada J. Heating values of wood pellets from different species. Biomass Bioenergy. 2011;35:2634−2639. [CrossRef]
[68] Bell I, Wronski J, Quoilin S, Lemort V.nPure and pseudo-pure fluid thermophysical property evaluation and the open-source thermophysical property library CoolProp. Ind Eng Chem Res 2014;53:2498−2508. [CrossRef]
[69] Dow Chemical. Dowtherm Q Technical Data Sheet. Last Accessed Date: 23.12.2023. Available at: https://www.dow.com/en-us/pdp.dowtherm-q-heat-transfer-fluid.11233z.html#overview
[70] National Center for Biotechnology Information. U. S. National Library of Medicine. Last Accessed Date: 23.12.2023. Pubchem. Available at: https://pubchem.ncbi.nlm.nih.gov/